Cold Gas Clouds and Rotational Asymmetry in the Galactic Halos

Noraiz Tahir
Regn.#00000172883

A thesis submitted in partial fulfillment of the requirements for the degree of **Master of Science**

in

Physics

Supervised by: Prof Asghar Qadir

Department of Physics

School of Natural Sciences
National University of Sciences and Technology
H-12, Islamabad, Pakistan

Year 2018

FORM TH-4

National University of Sciences & Technology

MS THESIS WORK

We hereby recommend that the dissertation prepared under our supervision by: MR. NORAIZ TAHIR, Regn No. 00000172883 Titled: Cold Gas Clouds and Rotational Asymmetry in the Galactic Halos be accepted in partial fulfillment of the requirements for the award of **MS** degree.

Examination Committee Members

1. Name: DR. MUDASSIR ALI SHAH   Signature: _____

2. Name: DR. AEYSHA KHALIQUE   Signature: _____

External Examiner: DR. JAMEEL-UN-NABI   Signature: _____

Supervisor's Name PROF. ASGHAR QADIR   Signature: _____

_____
Head of Department

_____
02/01/19
Date

COUNTERSINGED

Date: 02/01/19

_____
Dean/Principal

THESIS ACCEPTANCE CERTIFICATE

Certified that final copy of MS thesis written by **Mr. Noraiz Tahir,** (Registration No. **00000172883**), of **School of Natural Sciences** has been vetted by undersigned, found complete in all respects as per NUST statutes/regulations, is free of plagiarism, errors, and mistakes and is accepted as partial fulfillment for award of MS/M.Phil degree. It is further certified that necessary amendments as pointed out by GEC members and external examiner of the scholar have also been incorporated in the said thesis.

Signature: _____

Name of Supervisor: Prof. Asghar Qadir _____

Date: _____ 02/01/19 _____

Signature (HoD): _____

Date: _____ 02/01/19 _____

Signature (Dean/Principal): _____

Date: 02/01/2019 _____

I commit this thesis to my family and my solitary closest companion my future spouse "Shanza Tahir", for nursing me with affections and love and their committed association for accomplishment in my life

Acknowledgements

Abstract

Rotation of various galactic objects and halos is a question that is difficult to address. The cosmic microwave background data has opened up a gateway to see the rotation of various nearby galaxies including Andromeda (M31), Triangulum (M33), Centaurus-A (NGC 5128), Bode's (M81), Cigar (M82), and Sombrero (M104) galaxy. The galactic halo rotation can be probed and may be ascribed to molecular hydrogen clouds populating the galactic halos, but it is not sure that these clouds are pure molecular hydrogen or there is some contamination of other heavier molecules or interstellar dust present in the interstellar medium. In order to address this issue, in the thesis, I am going to model these clouds taking all these possibilities into account by using the canonical ensemble distribution, to get the mass density profile of these clouds, in order to constrain the physical parameters such as mass, radius, and central density.

Contents

List of Publications

1. Tahir, N., De Paolis, F., Qadir, A., and Nucita, A.A., "Constraining baryons in the M31 halo by using Planck data", submitted to *International Journal of Modern Physics D*, (2018).

2. Tahir, N., De Paolis, F., Qadir, A., and Nucita, A.A., "Seeing the halos of the nearby spiral galaxies by Planck data", submitted to *Arabian Journal of Mathematics Special Issue*, (2018).

3. Qadir, A., Tahir, N., De Paolis, F., and Nucita, A.A., "Virial clouds explaining the rotational asymmetry in galactic halos", presented in 15th *Marcel Grossmann Meeting Rome Proceedings*, (2018).

4. De Paolis, F., Gurzadyan, V.G., Nucita, A.A., Gurzadyan, A., Qadir, A., Jetzer, Ph., Ingrosso, G., and Tahir, N., "Rotating baryonic dark halos vs Planck halo mapping", submitted to *European Physical Journal C*, (2018).

5. Qadir, A., Tahir, N., De Paolis, F., and Nucita, A.A., "Virial clouds explaining the rotational asymmetry in galactic halos", submitted to *Physical Review D*, (2018).

List of Figures

List of Tables

Chapter 1

Introduction

It was thought that all of the hydrogen present in the interstellar medium (ISM) disappeared during star formation (for details on ISM see Section 1.3.1). According to the standard cosmological model of the Universe, 70% of the Universe consists of dark energy, 25% of *cold dark matter* (CDM) and around 5% of baryons [1, 2]. Half of these baryons are visible and half of them are invisible, and cannot be detected. In what form these baryons are missing is *still* an open question. Many suggestions were proposed in different papers (see [3, 4, 5, 6, 7, 8]) to answer this question.

Assuming that some small fraction of primordial hydrogen was not swept away during star formation, it would have started to collapse due to gravitational instability[1], to form clouds. These clouds would keep on collapsing further subject to the virial theorem and continue radiating at the virial temperature, *provided it was above the cosmic microwave background* (CMB)(see Section 1.2) *temperature*, and become stable, i.e. it would not be able to radiate any more or absorb any further radiation [9]. How could one search for these clouds?

One suggestion was to look for γ-ray scintillation because of cosmic rays striking the clouds. The problem with this method was that it would so be far away that we could not know what causes the radiation. Indeed, γ-ray "carpets" were seen, and the

---

[1]The gravitational instability is the instability caused by the molecules in the ISM. The molecules attracts other molecules due to the self gravitation and the region becomes denser. These denser regions will attract other molecules with greater gravitational force and become more denser and denser, which will lead to the formation of gas clouds.

observation was viewed as typically unconvincing proof [10, 11, 12]. Another proposal was to search for a Doppler shift in the adjacent M31 galaxy, because of the rotation of the galactic disk and halo. The part of the halo rotating away from us should be red-shifted and the part rotating towards us should be blue-shifted. WMAP data of 2011, displayed the effects at a low level [13]. An objection was raised that the blue-shift could be due to hot spots. Yet shouldn't something be said about red-shift? It couldn't be *cold* spots. In 2014, Planck data was released and confirmed the effect in the M31 halo at an adequate accuracy. It helped not only to prove the asymmetry but also was very helpful in mapping the rotational dynamics of the M31 halo, in more detail [14]. From that point forward, the data was used to map the rotational dynamics of many other galaxies, including NGC 5128, M33, M81 and M82 [15, 16, 17, 18].

There is no doubt that the effect is present and is useful to study the rotational dynamics of galactic disks and halos. However, the observation of the prediction does not prove that the clouds are made of only molecules of hydrogen. Since there are other, heavier, molecules (e.g. interstellar dust see Section 1.3.4) in the ISM. It might be possible that there are clouds that are composed of H_2 molecules or only dust molecules, or there might be clouds with H_2 and dust present in different proportions. With a specific end goal to clarify this issue, we have to model these clouds. We have to take all these above possibilities into account, and see what diverse situations may occur. One could, then, estimate the amount of a *masking* or *mimicking* effect that could originate from other interstellar matter.

The plan of the thesis is as follows: In chapter 1, I will explain that how Astronomy was evolved in Astrophysics (Section 1.1). Then in Section 1.2, I will explain how the temperature asymmetry was detected, and how it was helpful for us in mapping the rotational dynamics. I will also explain galaxies and galactic halos (Section 1.3), ISM (Section 1.3.1), and the dark matter distribution in the galactic halos (Section 1.4), then in Section 1.6 and 1.7, the virial theorem and Doppler shift in relativity will be discussed. In Chapter 2, I will present the isothermal Lane-Emden model, assuming that these clouds contain just molecular hydrogen. Then I will try to estimate the mass density profile of these clouds by using the well known Lane-Emden equation (Section

2.1), which will give an estimate of mass and radius of these gas clouds. Next, I will use the widely adopted dark matter distribution models (NFW, Moore and Burkert model), to estimate the total mass of the M31 halo and, by using the total mass of the halo and mass of each cloud, I will try to estimate the total number of clouds in the M31 halo. In Section 2.3, I will try to estimate the filling factor of these clouds in the M31 halo. After estimating the filling factor, I will assume that the whole M31 halo is composed of these clouds, and I will estimate the rotational velocity of the M31 halo. To this end, I have modeled the gas clouds (pure molecular hydrogen clouds) and estimated the physical parameters (mass density, mass, and radius), in Chapter 3, I will explain the virial model. The chapter is divided into two parts: the single-fluid model (Section 3.2); the two-fluid model (Section 3.3). In the single fluid model, I will try to model the clouds using the canonical ensemble distribution, and Jeans criterion, with the possibility that they are entirely composed of pure molecular hydrogen or pure interstellar dust, and I will again try to estimate the physical parameters of these clouds. Then in the two-fluid model, I will try to model the other possibility and will estimate the physical parameters of the clouds, if they have different fractions of molecular hydrogen and dust in them by again using the canonical ensemble distribution and Jeans criterion. This is the thing that we are extremely intrigued to determine. Toward the end, in Chapter 4, the results and conclusions will be discussed.

1.1   Evolution of Astronomy

The Universe contains numerous celestial objects, and the study of these objects is Astronomy, while Astrology is the study of relating the development of these heavenly objects on human life. By the beginning of ∼5000 BCE, many Astronomers began to assemble sun observatories. Stonehenge was one of these observatories which was developed, almost, in the middle of 3100-2000 BCE [19].

The Nile is one of the major rivers flowing in North Africa. The flooding of the Nile destroyed the crops of the Egyptians, so, they used stars to keep records of the seasons, to plant the crops. In this way, Astronomy began to develop in ∼3000 BCE

in Egypt. Till, around the 21st to 22nd BC, Astronomy stayed attached to Astrology, and it wasn't before the end of around 600 BCE, and onwards that the Greeks, turned Astronomy, from minor perceptions to being a theoretical science, worried about the structure of the Universe.

In around the 4th century BC, Plato worked with his student Aristotle, on a geocentric model of the Universe. They proposed that the Earth is at the center of the Universe and is stationary. The Stars and the Planets move in circles around the Earth which are arranged in the order as Moon, Sun, Venus, Mercury, Mars, Jupiter, Saturn, fixed stars, with the fixed stars located on the celestial sphere. Claudius Ptolemy a Greco-Roman mathematician and astronomer, refined the geocentric model by introducing epicycles and deferents. He explained this concept of the modified geocentric model of the Universe with epicycles and deferents in his book "*Almagest*", which was used by the Western world for around 1500 years. Aristarchus in around 280 BCE, proposed a heliocentric model (Sun centered theory) of the Universe, but his theory was not largely acknowledged then, because the model became a part of the Christianity at that time.

Astronomy started to come to fruition during the *Renaissance*. It began as a social development in Italy and later spread to whatever was left of Europe. In 1543, Nicolaus Copernicus a Polish-German mathematician and astronomer, published his "*De Revolutionibus Orbium Coelestium*", and reviewed the heliocentric model of the Universe, which was first proposed by Aristarchus. Interestingly, he published his book when he was on his death bed, because the Christians around then had a strong belief, in the Earth centered theory, and anyone who rejected it, was condemned to death.

Not long after Copernicus's death, in the last part of the 16th century, Tycho Brahe a Danish astronomer, started to observe Mars, and numerous other planets. He made an observatory on an island in Denmark, where he used mammoth sized telescopes to observe the Planets. Not long after Tycho lost his money, he moved to Prague for his later work. After some time a youthful colleague, Johannes Kepler, came in his observatory. Kepler started working with Brahe on planetary observations in the laboratory. Tycho Brahe died in around 1605, and four years after his death, Kepler

deduced that the Planets move in elliptical orbits around the Sun, and he proposed three laws to explain their motion. These are known as Kepler's Law of Planetary Motion.

<center>(a)   (b)</center>
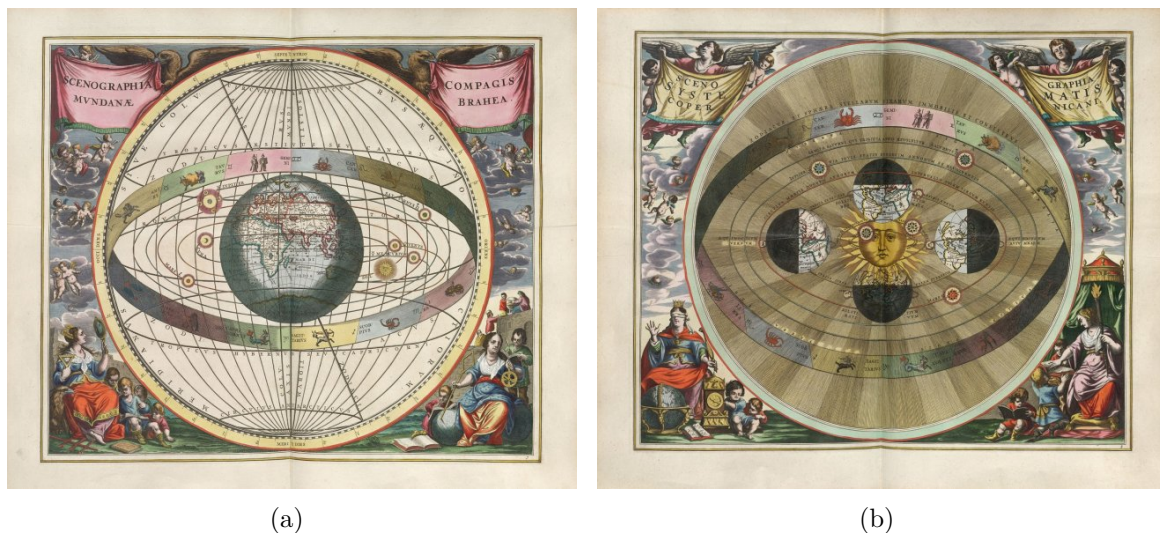
Figure 1.1: Fig.1.1(a) a geocentric universe depicted in 1660, and Fig.1.1(b) a heliocentric universe depicted in 1660 (Credit: The Harmoniamacrocosmica of Andreas Cellarius. Public domain.).

Galileo Galilei, an Italian astronomer and physicist at that point added to the developing group of logical astronomical information, by using his recently made telescope to observe Jupiter's spinning moon system. He said that with his telescope he could see more stars than he could with his naked eye and could see the Milky Way. He portrayed the surface of the Moon and mapped the mountains, pits and the dark spots on it, which he called "*maria*" (for seas). He additionally proved that Saturn had a more perplexing shape than that of a sphere, by using his telescope. He likewise found the Sunspots and predicted their movement on the Sun. Galileo was not able to advance his work, because the Church resisted him. They thought that he could take his research to a religious level.

At that point came the English scientist, Sir Issac Newton. He played a key role in the advancement of physics, mathematics and astronomy. His book, "Philosophiae Naturalis Principia Mathematica (Mathematical Principles of Natural Philosophy)",

<center>5</center>

| (a) | (b) |
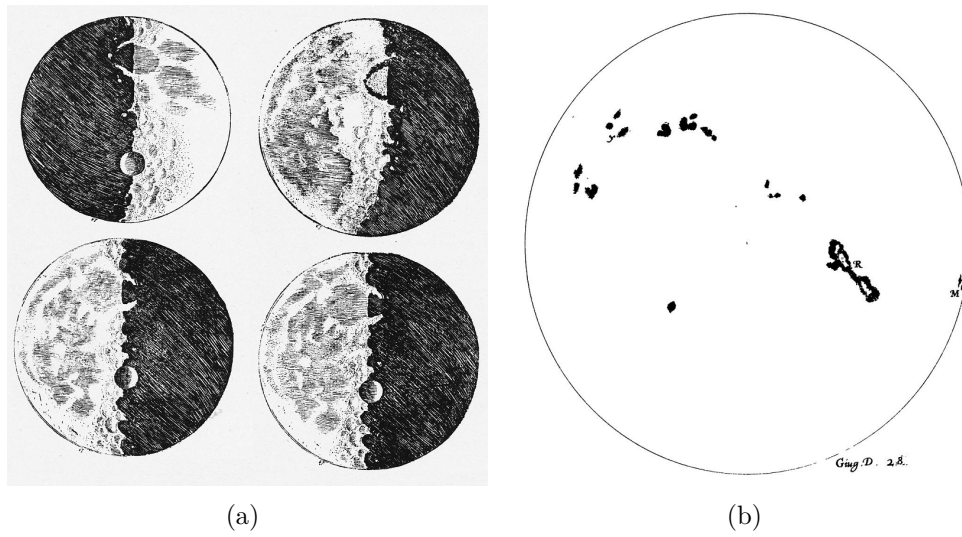
Figure 1.2: Fig.1.2(a) A sketch of the Moon by Galileo from Sidereus Nuncius, 1610, and Fig.1.2(b) Sketches of the sunspots by Galileo from Istoria e Dimostrazioni Intorno Alle Macchie Solari e Loro Accidenti Rome, 1613 (Credits: Galileo Galilei. Public domain.).

shortened to "Principia", was first published in 1687, and later translated in English by Andrew Motte in 1729, laid the foundations of Classical Mechanics. In his book, he formulated his *three laws of motion* [20], which were derived from Johann Kepler's Laws of Planetary Motion, and his own mathematical explanation of gravity. He also formulated his *Law of Universal Gravitation* in the Principia, which states that "Every body in the Universe attracts every other body with a force that is proportional to the product of their masses and inversely proportional to the square of the distance between them" [20]. He used his mathematical descriptions to explain the motion of comets, the tides, and many other astronomical phenomenas.

The observations of heavens beyond the Milky Way began in 1700s by William Herschel. In the 1780s, an English natural philosopher John Michell came up with a method to work out the masses of stars. In coming up with the idea, he imagined a case where the gravitational pull of a star becomes extremely strong that even light can not escape through it. That's how, in 1783, he came up with an idea that would eventually be called *black holes*. At that time, it was not yet known that there is nothing faster

6

than the speed of light, but this detail did not matter for him. The crucial point was that, because light could not escape the star, the star would be invisible to all outside observers. He named them **"dark stars"** [21]. A few years later, in around 1798, Laplace also proposed the idea of these dark stars [21].

In the 19th century astronomers started to investigate more not only about the positions and motion of the celestial phenomenas and objects, but also the physics of these phenomenas and objects. The use of stellar spectroscopy by William Huggins in studying the nature of the many nebulous objects in the sky lead the way to astrophotography, which helped in discovering numerous other astronomical objects. In 1817 Charles Messier assembled around 103 significant astronomical objects called "Messier objects", as not comets, which included nebulae, star groups and galaxies [22].

Max Planck's realization that energy is quantized in 1901, led to the discovery of Quantum Mechanics, and Albert Einstein's theory of Special Relativity (SR) in 1905 and theory of General Relativity (GR) in 1915, changed the manner in which the structure of spacetime, and gravity were seen. Observational astronomy has grown exponentially ever since, and this was the beginning of its evolution to astrophysics.

1.1.1 Einstein: A Static Universe

In 1917, German-Swiss-American physicist Albert Einstein attempted the first relativistic model of the Universe, in order to test his GR. He wrote a letter to the Dutch Astronomer Willem de Sitter saying *"For me...it was a burning question whether the relativity concept can be followed through to the finish, or whether it leads to contradictions"* [23]. He solved his field equation, and found that the covariant field equations of relativity gave a solution corresponding to an expanding Universe. He was not convinced by the results, because at that time it was a belief that the Universe is eternal. So, he modified his field equations by adding a "cosmological constant", and showed that the modified field equations gave the solution for a static universe. His model of the cosmos gave a satisfactory relation between the size of the Universe and the amount of matter it contained. Indeed, he also attempted a rough estimate for the

size of the Universe at that time, using estimates of the density of matter in the Milky Way, although he later realised that such calculations were unreliable [24].

In the 1920's the Russian mathematician, Alexander Friedmann and the French Priest Georges Lemaitre proposed that spacetime could be expanding, or contracting [25], by solving the Einstein's field equations without the cosmological constant. Soon this was observed by Hubble, in 1929 (see Section 1.1.2). Einstein was one of the first to accept Hubble's observations as likely evidence of a non-static Universe. In April 1931, Einstein published a model of the expanding cosmos of a matter-filled dynamic Universe of positive spatial curvature [26]. The most important feature of the Friedman-Einstein model, was that Einstein dispensed with the cosmological constant term for two stated reasons: first, the term was unnecessary because the assumption of static universe was no longer justified by observation; second, the term does not provide a stable static solution for the Universe. Einstein got the solutions in his first attempt to solve his field equations, without the cosmological constant, but then he was not convinced by the solution of an expanding Universe. That's why he calls it the "biggest blunder" of his life. In a substantial article on the 'Big Bang' model of the evolution of the Universe published in *Scientific American* in May 1956 [27], Russian emigre physicist George Gamow wrote: *"Studying Einstein's publications on that subject from a purely mathematical point of view, Friedmann noticed that Einstein had made a mistake in the alleged proof that the Universe must necessarily be stable and unchangeable in time. Einstein's proof does not hold and Friedmann realised that this opened up an entire world of time-dependent universes: expanding, collapsing, and pulsating ones. Thus, Einstein's original gravity equation was correct, and changing it was a mistake. Much later, when I was discussing cosmological problems with Einstein, he remarked that the introduction of the cosmological term was the* **biggest blunder** *he ever made in his life. But this "blunder", rejected by Einstein, is still used by cosmologists even today, and the cosmological constant denoted by the Greek letter Λ raises its ugly head again and again and again"* [28].

1.1.2   Hubble Again: An Expanding Universe

Edwin Hubble in 1929 attempted to see whether spacetime is expanding or contracting by estimating the Doppler shift of light (discussed in Section 1.7) from galaxies at different distances, keeping in mind the end goal to see which are moving towards us and which are moving away from us [29].

In order to gauge the distance to the galaxies, Hubble used a strategy discovered by an American Astronomer Henrietta Swan Leavitt. Leavitt demonstrated that there is a relationship between the pulsation period of specific kinds of stars, and their natural luminosity [30]. She showed that the intrinsic luminosity of a star can be used to determine how bright it would as compared to the Sun. This technique was then used by the researchers to estimate how far away the star must be. Leavitt was not able to make use of her discovery, since, females were not allowed to use high-gauge telescopes until the 1960s. By using the method proposed by Leavitt, Hubble demonstrated that on a large enough scale, our observations are the representation of the whole Universe and the Universe is the same in all directions. He was able to determine the velocity at which the galaxies are moving away using spectroscopy. He found that almost every galaxy is red-shifted, which means that almost every galaxy is moving away from us. He also found out that older, galaxies seem, to be moving separately at a higher velocity than newer ones.

1.1.3   Other Possibilities of the Universe

Since the Universe is expanding, there are three possible outcomes for how the Universe will look like and how it will end.

- If the force of gravity is more than the force of expansion, so the Universe will re-collapse in a 'Big Crunch'. This is known as a *Closed Universe.*

- If the force of gravity is equal to the force of expansion, so the Universe will achieve a most extreme size and will expand much. This is known as a *Flat Universe.*

- If the force of expansion is more than the force of gravity, the Universe will keep on expanding until the end of time. This is known as an *Open Universe*. This is the possibility that Hubble accepted.

Einstein demonstrated that spacetime is moulded by mass, thus Open, Flat, and Closed Universes will have distinctive shapes [31]. The state of the Universe relies upon the density parameter '$\Omega_0 = \rho/\rho_{crit}$'. This is a measure of the actual density of the Universe, ρ, to the critical energy density, ρ_{crit}. An expression for the critical density is found by assuming Λ to be zero (as it is for all basic Friedmann universes) and setting the normalised spatial curvature, k, equal to zero. When the substitutions are applied to the first of the Friedmann equations we find $\rho_{crit} = 3H^2/8\pi G$.

- In an open Universe, $\Omega_0 < 1$, and spacetime is curved inwards, similar to the base of a seat.

- In a flat Universe, $\Omega_0 = 1$, and spacetime is flat, similar to a sheet of paper.

- In a closed Universe, $\Omega_0 > 1$, and spacetime is curved outwards, similar to a circle.

1.1.4   A Brief History of the Universe

The Big Bang Theory is the explanation about how the Universe began. According to the theory, the Universe was an unimaginably hot, dense point, before its birth, and then it started expanding. The "echo" of this expansion known as the CMB can be observed (see Section 1.2).

In the first second after the Universe began, the surrounding temperature was about 10^{10} ^{0}F. At that time the Universe contained a vast number of fundamental particles, they decayed and combined as the Universe got cooler. As the Universe continued to decrease in density and temperature, the energy of each particle began to decrease. Since, the temperature was not very high, mass annihilation occurred immediately. Atomic nuclei were made inside 3 minutes of the Big Bang. American physicists George
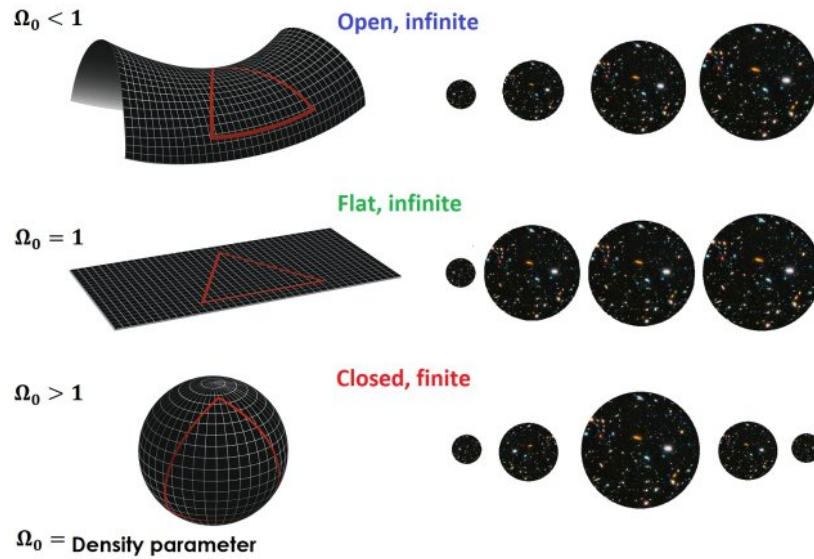
Figure 1.3: The left hand side of the figure gives different possibilities of the shape of spacetime for different density parameters. The right hand side of the figure explains that how the expansion will look corresponding to each state of the Universe; for $\Omega_0 < 1$, the Universe will expand at a constant rate forever; for $\Omega_0 = 1$, the Universe will expand forever, but the rat of expansion is not constant it is decreasing with time; for $\Omega_0 > 1$, the spacetime is curved outwards, the Universe first expands at a constant rate and then after a certain time it will re-collapse in a Big Crunch. (Credits: Modified by Helen Klus, http://www.thestargarden.co.uk/Big-bang.html, original images by NASA and NASA/Hubble. Public domain.).

Gamow, and Ralph Alpher explained how this happened, in a procedure known as Big Bang Nucleosynthesis, in 1948 [32]. After $380,000$ years, the Universe got cool enough that the electrons combined with nuclei to form atoms mostly hydrogen and helium. This procedure is known as recombination. After recombination, the radiation decoupled from matter and continued to expand through space. This radiation is the CMB. German-American physicist Hans Bethe [33], and Indian-American physicist Subrahmanyan Chandrasekhar [34], explained that how stars are fuelled by atomic combination in 1939. Two American electrical engineers, Arno Penzias and Robert Woodrow Wilson incidentally observed and discovered Gamow and Alpher's, CMB, in 1964 [35, 36]. This gave the proof that the Big Bang Theory is right.

In 1984, physicists George Blumenthal, Sandra Moore Faber, Joel Primack, and

Martin Rees showed that small objects like stars formed before larger objects like galaxies and galaxy clusters [37]. The first stars are thought to be formed around 200 million years after the Big Bang [38], and planets started to shape when the first generation of stars died following a couple of million years. The first galaxies were formed inside 400 million years after the Big Bang.

The oldest Stars in the Milky Way are more than 13 billion years old, yet it is believed that the disk of the Galaxy was formed around 9 billion years ago [39]. The Solar System, was formed around 4.6 billion years ago, around 9.2 billion years after the Big Bang.

1.2   Detection of the Cosmic Microwave Background

On November 18, 1989 NASA's Cosmic Background Explorer (COBE) left the Earth's orbit, and revolutionized our understanding of the early Universe. The satellite was created and worked at Goddard Space Flight Center, in Greenbelt. COBE mapped the oldest light in the Universe, also known as the CMB. It was observed that there were a few fluctuations, or ripples, in the temperature of the Universe. The mission took us into another era of precision measurements, preparing for more accurate measurement of the CMB.

The mission was then followed by NASA's Wilkinson Microwave Anisotropy Probe Mission (WMAP). WMAP space mission completed its measurements, in nine long years. The satellite not just gave a more accurate measurement of the CMB, it also gave us an estimate of the age of the Universe and the formation of the vast structure like galaxies. It gave better details at the temperature asymmetry in the CMB. It is also in the Guinness Book of World Records for "the most precise measure of the age of the Universe". The mission estimated that the Universe is, 13.75 billion years old, with a degree of error of about 1%. WMAP also confirmed the existence, of dark energy and explained that it fills 72% of the Universe. The satellite was Launched as, MAP on June 30, 2001 and later renamed as WMAP. After WMAP European Space Agency's (ESA's), Planck satellite was launched in 2009, and gathered the data till, 2013. It
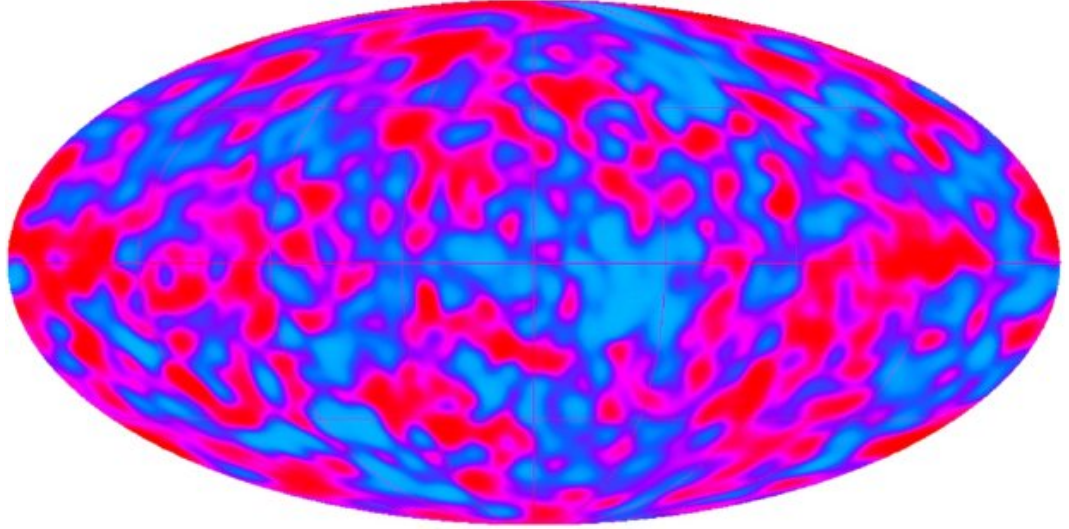
Figure 1.4: This image, is the map of the CMB found by the four years COBE data. It was gathered somewhere in between 1990 and 1992, got much attention at the time. The map demonstrates temperature fluctuations in the Universe (shown as color difference). (Credits: NASA. Public domain)

was based only, on the observation of the temperature of the CMB. It gave us the best and precise confirmation about the temperature asymmetry in the CMB. Other than mapping the temperature of the CMB, over the sky with exceptional precision, Planck additionally estimated its polarization.

1.3 Galaxies and Galactic Halos

The galactic halos are the extended parts of a galaxy, which goes past our noticeable segment. They are divided into three parts: stellar halos, galactic coronas, and dark matter halo. A stellar halo contains the number of inhabitants in the form of stars, and globular clusters, this part contains the fossils of the formation of the galaxies, the part of the halo can be used to study the formation of galaxies, and it is been done for the M31, and the Milky Way [40, 41]. The galactic corona, contains hot, & ionized gases (plasma). The dark matter halo is the theoretical distribution of dark matter, in the galactic halos (see Section 1.4).
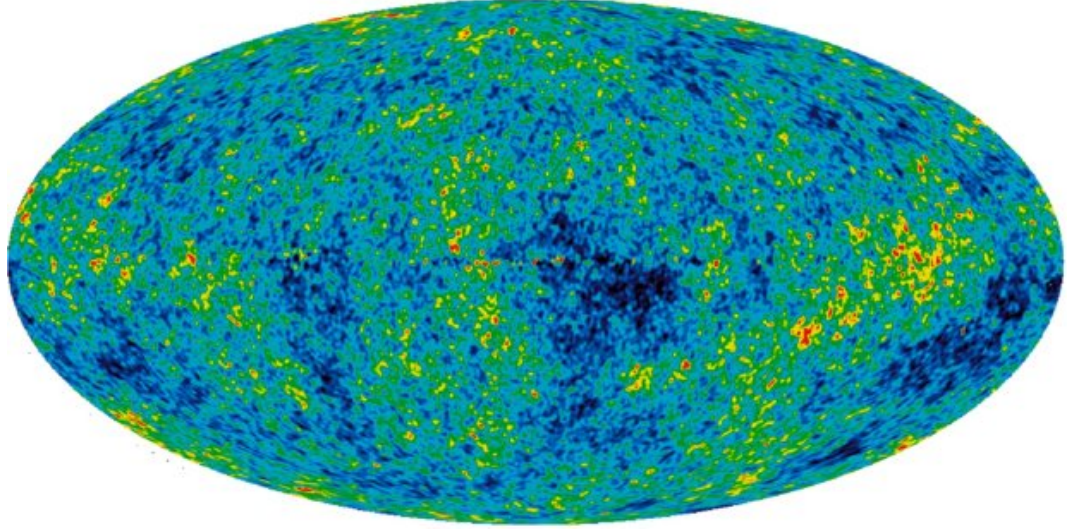
Figure 1.5: This picture is the definite, all sky map of the Universe made from seven long years of WMAP data. The figure uncovers 13.7 billion year old temperature asymmetry (Credit:NASA).

1.3.1 Interstellar Medium

ISM is the space between the Stars which is filled with particles, molecules, atoms, and interstellar dust grains. Galaxy formation and its evolution, the arrangement of stars, cosmic nucleosynthesis, the origin of large complex, prebiotic molecules and the plenitude, structure, and formation of interstellar dust grains, these physical processes are occurring in the ISM [42].

ISM consists around 90% hydrogen, 9% helium in addition to heavier components, e.g. interstellar dust [43]. There are singular and individual clouds of dust and gases, these clouds are named as "nebulae". The gases in the ISM are found to have different temperatures, densities, and ionization states altogether. The pressure, density, and temperature of the gas in the ISM are explained by the perfect gas law. For a volume, V, pressure, P, and absolute temperature, T, we have the perfect gas law as

$$PV = N_p kT = N_{mole} RT, \tag{1.1}$$

where, k is the Boltzmann constant, N_p is the total number of particles, R is known as the perfect gas constant, and N_{mole} is the number of moles in the volume.

14
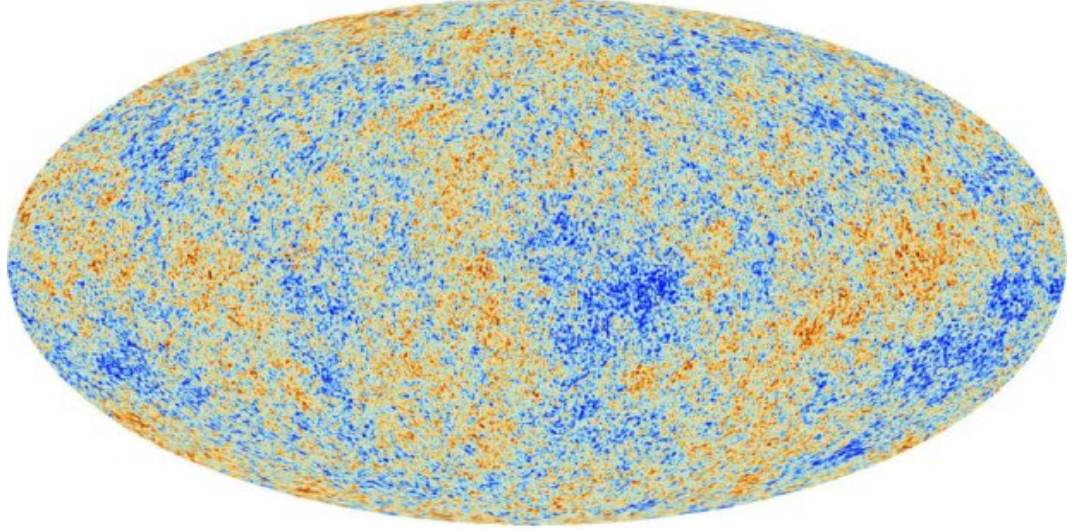
Figure 1.6: Planck map of the CMB, showing temperature fluctuations in the Universe (Credits: ESA and the Planck Collaboration).

1.3.2 Components of the Interstellar Medium

It is important to distinguish the ISM into different other mediums, these are called phases [44]:

1. The cold neutral medium, consists of neutral hydrogen (H_I), and other molecules at temperatures, $T \sim 10 - 100$K, and high densities.

2. The warm neutral medium, contains, H_I, but at, $T \sim 10^3 - 10^4$K, and low densities.

3. The warm ionized medium, consists of ionized gas (H_{II}) at temperatures, $T \sim 10^4$K, and of lower densities.

4. The hot ionized medium, consists of ionized gas (H_{II}) at very high temperatures, $T \sim 10^5 - 10^6$K, but very low densities.

5. The cold dense medium, contains molecular gas, mostly, H_2, at very low temperature, $T \leq 10$K, and very high densities.

1.3.3 Cold Dense Regions of the Interstellar Medium

The cold regions of ISM, contain large amount of molecular hydrogen (H_2). H_2 is difficult to detect, as it has no radio lines, in order to detect the gases in ISM these radio lines are observed, since, they keeps the coldest, and densest parts of the ISM being seen, straightforwardly. Different particles (other than H_2) emits lines in the radio region, these molecules emit these lines because of the transfer of energy of the molecules. The energy transfer can be because of changes in the electron energy levels, and due to the change in vibrational and rotational energies of the molecules. Each of the three energies are quantized. Transitions between the vibrational states can produce lines in the infrared region. Transitions between the rotational states are in general the least energetic, and emit lines in the radio region. Carbon monoxide (CO) has strong radio lines at 1.3 mm, and 2.6 mm, from transitions between rotational states, hence, it is valuable as a tracer of H_2 molecules, with a fact that the densities of these two are corresponding. Mapping CO distribution is used to map the distribution of cold gas in the ISM. Cold molecular gas is in the form of molecular clouds. These are generally small in size about $\simeq 2 - 40$pc, having temperature $\leq 10K$, and number densities $\sim 10^8 - 10^{11} m^{-3}$ [45]. Molecular clouds fill just a small space of the ISM, however, they have smaller masses. Portions of gas in molecular clouds can encounter collapse due to self gravitation in order to form stars. The recently formed hot stars thus illuminate the gas with ultraviolet light, ionizing, and warming the gases [46, 47]. ISM also contain giant molecular clouds (GMCs). They are bigger colonies, of cold molecular gases, having sufficiently larger masses of about $106 M_\odot$. Inside our Galaxy, they are found in its spiral arms [48].

1.3.4 Interstellar Dust

Interstellar dust consists of silicates, and carbon mixes. The biggest is $\simeq 0.5$ μm, with $\sim 10^4$ atoms. However, some of the interstellar dust grains seem to have $\lesssim 10^2$ atoms [49, 50]. They have a significant observational impact, it absorbs all the scattered light. Dust also lessens the light of background sources, this procedure is known as

interstellar extinction, dark nebulae is one of its examples [51].

Consider, light of wavelength, λ, with a particular intensity, I_λ, going through ISM. If the light goes through a component of length in the ISM, it will encounter a change, dI_λ, in the intensity, I_λ, because of absorption, and scattering by dust. This is identified with the change, $d\tau_\lambda$, in the optical depth, τ_λ, at the wavelength, λ that the light encounters along its travel by

$$\frac{dI_\lambda}{I_\lambda} = -d\tau_\lambda, \tag{1.2}$$

Integrating, over the line of sight from a light source to an observer, the observed intensity is

$$I_\lambda = I_{\lambda_0} exp\left(-\tau_\lambda\right), \tag{1.3}$$

where, I_{λ_0} is the light intensity at the source, and τ_λ is the average optical depth along the line of sight.

Dust also causes excitation in the galaxies. The excitation turns out to be extremely strong for long range lines through the disc of the Galaxy. The Galactic center is totally misty to optical perceptions. Couple of regions of lower dust excitation towards the bulge of our Galaxy (e.g. Baade's Window), empower the stars in the bulge and are studied [52]. We can estimate the excitation caused by dust in the Galaxy to see, how the value of excitation towards the distant galaxies change with the galactic latitude, b. The optical depth caused by dust excitation when light of wavelength, λ, travels a short distance, ds, in the ISM is given by, $d\tau_\lambda = \kappa_\lambda \rho_d ds$, where, ρ_d is the density of the single interstellar dust grain, and κ_λ, is the mass excitation coefficient for λ. Estimation of the Star numbers, show that their number density decays exponentially with distance from the Galactic plane [53]. Let the density of dust changes with separation, z over the Galactic plane then the density will be given as $\rho_d(z) = \rho_{d_0} exp\left(-|z|/h\right)$, where, ρ_{d_0}, and h, are constants.

1.4 Dark Matter Distribution in the Galactic Halos

A dark matter halo of a galaxy starts from the galactic disc and expands well past the edge of the visible galaxy. The mass of the dark matter halo is more than the total mass of the galaxy. They can not be observed directly. This part of the halo plays a key part in the current models of galaxy formation, and evolution (for details see [54, 55]). The dark matter distribution, in the galactic halo, is generally described by using different models.

1.4.1 Einasto Model

The Einasto model is a mathematical distribution that explains, how the density, ρ, of a spherical astronomical object varies with distance, r, from its center. Jaan Einasto, presented his model at a 1963 meeting, in Alma-Ata, Kazakhstan [56]. The density profile is given by the relation

$$\rho_{Einasto}(a) = \rho_c exp\left(-d_N\left(\left(\frac{a}{a_c}\right)^{1/N} - 1\right)\right),\tag{1.4}$$

where, d_N is a function of N (the total number of particles), ρ_c is the central density, $a = \sqrt{r^2 + z^2/q^2}$ is the distance from the center, and similarly, a_c is related to the central distance, r_c. The parameters ρ_c, and r_c, are constant. They vary from halo to halo.

1.4.2 Navarro−Frenk−White Model

The Navarro−Frenk−White (NFW) model is a spatial mass distribution of dark matter fitted to dark matter halos, identified in N-body simulations, by Julio Navarro, Carlos Frenk, and Simon White [57]. It is the most normally used profile to show the dark matter distribution, in the halos. The profile is given by

$$\rho_{NFW}(r) = \frac{\rho_c}{\left(\frac{r}{r_c}\right)\left(1 + \frac{r}{r_c}\right)^2}.\tag{1.5}$$

1.4.3 Moore Model

The model is used to explain the CDM distribution in the halos. It is the best model to explain the distribution of CDM [58]. The density profile is given by

$$\rho_{Moore}(r) = \frac{\rho_c}{\left(\frac{r}{r_c}\right)^{3/2}\left(1 + \left(\frac{r}{r_c}\right)^{3/2}\right)}.$$

(1.6)

1.4.4 Burkert Model

The Burkert model explains the observed rotation curves of dwarf galaxies, which are known to be filled with dark matter all through. The Burkert profile is an exact profile that looks exactly like a pseudol-isothermal halo. Rather than the CDM profiles, it likewise has a core, and is explained by the central radius, r_c, and by the central density, ρ_c. The density profile is given by

$$\rho_{Burkert}(r) = \frac{\rho_c}{\left(1 + \frac{r}{r_c}\right)\left(1 + \left(\frac{r}{r_c}\right)^2\right)}.$$

(1.7)

1.5 Ensembles in Thermodynamics

There are three types of ensembles in thermodynamics: micro canonical; canonical; and grand canonical ensemble [59].

A micro canonical ensemble represents, the possible states of a mechanical system having the exactly specified energy. The entropy of the system is given by the relation

$$S = -k \sum_{\nu=1}^{W} \left(\frac{1}{W}\right) ln\left(\frac{1}{W}\right) = kln(W),$$

(1.8)

where, k is the Boltzmann constant, $\sum f_\nu = 1/W$, and f_ν is the distribution of particles in the system. The probability distribution for a micro canonical ensemble is given by the relation

$$P_{micro} = \frac{1}{h^\phi N!}\frac{1}{W}f\left(\frac{H-E}{\omega}\right).$$

(1.9)

19

Here, $\phi = 3N$ is the degrees of freedom, H is the Hamiltonian, E is the energy of the system, ω is the frequency of the particles in the system. W is determined by

$$\int \int \frac{1}{h^\phi N!} exp\left(-\pi \left(\frac{H-E}{\omega}\right)^2\right) dp_\phi \ldots dq_\phi, \tag{1.10}$$

A canonical ensemble is the one that represents the possible states of a mechanical system, in thermal equilibrium with a heat bath at a fixed temperature. The system can exchange energy with the heat bath, so that the states of the system will differ in total energy. If we work out an ensemble in which the temperature is fixed, then we don't need to minimize $U - TS$ (where, U is the internal energy, S is the entropy and T is the temperature.) to obtain U, and S, as a function of temperature, T. The distribution for a canonical ensemble is

$$f(r,p) = \frac{1}{h^\phi N!} \frac{1}{Z} exp\left(-\frac{H(r,p)}{kT}\right), \tag{1.11}$$

where, Z is the partition function which is defined as

$$Z = \frac{1}{h^{3N} N!} \int \int dp \ dr \ exp(\frac{-H(r,p)}{kT}). \tag{1.12}$$

If we have more than one fluids in contact with the heat bath we can write the partition function for the whole system as

$$Z = Z_1.Z_2.Z_3\ldots. \tag{1.13}$$

So,

$$Z = \frac{1}{h^{3(N_1+N_2+N_3\ldots)} N_1!N_2!N_3!\ldots} \int \int dp \ dr \ exp\left(\sum_{i=1}^\phi \frac{H_i(r,p)}{kT}\right). \tag{1.14}$$

Grand canonical ensemble is that which is used to represent the possible states of a mechanical system of particles that are being maintained in thermodynamic equilibrium with a reservoir. The system can exchange energy, and also particles with the reservoir, so that various possible states of the system can differ in both their total energy, and in total number of particles. The probability distribution is

$$P_{grand} = \frac{1}{h^\phi N!} exp\left(\frac{\Omega + \sum_{i=1}^\phi \mu_i N_i - E}{kT}\right), \tag{1.15}$$

where, Ω is the grand potential, and μ is the chemical potential.

We are now able to understand the concept of the ensembles and the probability distributions that are associated with each ensemble. Since, we have to estimate the Jeans criterion of gravitational collapse for the clouds. We need to understand a general theorem, which helps us to get various information about stars, stellar structures, and interstellar gas clouds, this is the virial theorem. In this section, I will explain it for the clouds, when they are without magnetic field, and when they have magnetic field [60].

1.6 Virial Theorem

1.6.1 Virial Theorem for Clouds without Magnetic Field

Consider, a system of point particles, with position vectors as $\vec{x_i}$, the force applied on the particles is, $\vec{F_i}$, then the equation of motion for the i-th particle can be written as

$$\frac{d\vec{p_i}}{dt} = \vec{F_i},\tag{1.16}$$

where, $\vec{p_i}$ the momentum of point particles. Let us consider a scalar quantity

$$G = \sum_{i=1}^{N} \vec{p_i}.\vec{x_i}.\tag{1.17}$$

The summation in eq.(1.17) is all over the particles in the system. Taking the time derivative of the above scalar we will have

$$\frac{dG}{dt} = \sum_{i=1}^{N} \frac{d\vec{x_i}}{dt}.\vec{p_i} + \sum_{i=1}^{N} \frac{d\vec{p_i}}{dt}.\vec{x_i}.\tag{1.18}$$

Substitute $p_i = m_i.(dx_i/dt)$ in first term, and from eq.(1.17) we can rewritten as

$$\frac{d}{dt} \sum_{i=1}^{N} \vec{p_i}.\vec{x_i} = \sum_{i=1}^{N} m_i \frac{d\vec{x_i}}{dt}.\frac{d\vec{x_i}}{dt} + \sum_{i=1}^{N} \vec{F_i}.\vec{x_i}.\tag{1.19}$$

The above equation can be reduced to

$$\frac{d}{dt} \sum_{i=1}^{N} \vec{p_i}.\vec{x_i} = 2K + \sum_{i=1}^{N} \vec{F_i}.\vec{x_i},\tag{1.20}$$

where,

$$K = \frac{1}{2} \sum_{i=1}^{N} m_i \vec{v_i}^2 = \frac{1}{2} \sum_{i=1}^{N} m_i \frac{d\vec{x_i}}{dt}.\frac{d\vec{x_i}}{dt}. \tag{1.21}$$

The kinetic energy is due to the motion of particles in the system. In our case there is the thermal motion of particles, so, we should need the thermal kinetic energy which is given as

$$K = \frac{3}{2}kT, \tag{1.22}$$

where, $k = 1.38 \times 10^{-23} \mathrm{m}^2$ kg s^{-2} K^{-1} is the Boltzmann constant and T is the temperature. Time average of eq.(1.20), over the time interval τ is obtained by integrating both sides with respect to t from 0 to τ and dividing by τ which yields

$$\frac{1}{\tau} \int_0^\tau \frac{dG}{dt} dt = \left\langle \frac{dG}{dt} \right\rangle = \langle 2K \rangle + \left\langle \sum_{i=1}^{N} \vec{F_i}.\vec{x_i} \right\rangle, \tag{1.23}$$

or

$$\langle 2K \rangle + \left\langle \sum_{i=1}^{N} \vec{F_i}.\vec{x_i} \right\rangle = \frac{1}{\tau} \left(G(\tau) - G(0) \right). \tag{1.24}$$

If the motion is periodic, i.e. all coordinates repeat after a certain interval of time and also τ is chosen to be the period then right hand side of eq.(1.23), is zero. If the motion is not periodic provided the coordinates and the velocities of all particles remain finite so that there is an upper bound to G then by choosing τ to be sufficiently large, right hand side of eq.(1.24) can be made small as desired. Hence, we will get eq.(1.24) as

$$\langle 2K \rangle + \left\langle \sum_{i=1}^{N} \vec{F_i}.\vec{x_i} \right\rangle = 0. \tag{1.25}$$

This is the general mathematical form for virial theorem. The second part in eq.(1.25) on the left side is the potential energy. In this form it is important in kinetic theory of gases as it can be used to derive ideal gas law for perfect gases. We have considered a case when the clouds have no magnetic field, but in ISM there are clouds that will have a magnetic field in them. So the virial theorem will change for these clouds.

1.6.2 Virial Theorem for Clouds with Magnetic Field

Magnetic field is known to be an important constituent of astrophysical systems, so, we will include magnetic field in our derivation. Consider a system occupying a volume V and there is a constant magnetic field $\vec{B}$. Also consider that the force acting on the particles is due to the gradient of pressure P, i.e. $\vec{F} = \vec{\nabla} P$, the magnetic field and the gravitational pull of particles. The equation of continuity is given by

$$\frac{\partial n}{\partial t} + \vec{\nabla}.(n\vec{v}) = 0. \tag{1.26}$$

The equation of motion is

$$\rho \frac{\partial \vec{v}}{\partial t} + \rho \left(\vec{v}.\vec{\nabla} \right) \vec{v} = nq \left(\vec{E} + \vec{v} \times \vec{B} \right) - \vec{\nabla} P. \tag{1.27}$$

Substituting, $nq = \rho_q$, and $\rho = \rho_m$ in eq.(1.27). $\vec{v}.\vec{\nabla}$, makes the second term in the above equation zero, because the motion of particles is perpendicular to the gradient. Hence,

$$\rho_m \left(\frac{\partial \vec{v}}{\partial t} \right) = \rho_q \left(\vec{E} + \vec{v} \times \vec{B} \right) - \vec{\nabla} P. \tag{1.28}$$

As, $nq\vec{v} = \vec{j}$ and $\vec{E} = -\vec{\nabla}\phi$, so, we have the above equation as

$$\rho_m (\frac{\partial \vec{v}}{\partial t}) = -\vec{\nabla} P + \vec{j} \times \vec{B} - \rho_q \vec{\nabla}\phi. \tag{1.29}$$

Substituting,

$$\vec{j} = \frac{1}{4\pi} \left(\vec{\nabla} \times \vec{B} \right), \tag{1.30}$$

we have eq.(1.29) as

$$\rho_m \left(\frac{\partial \vec{v}}{\partial t} \right) = -\rho_q \vec{\nabla}\phi + \frac{1}{4\pi} \left(\vec{\nabla} \times \vec{B} \right) \times \vec{B} - \vec{\nabla} P. \tag{1.31}$$

Now,

$$
\begin{aligned}
[(\vec{\nabla} \times \vec{B}) \times \vec{B}]_l, \quad &= \quad \epsilon^{ijk} \partial_j B_k \epsilon_{lim} B^m, \\
&= \quad -\epsilon^{ijk} \epsilon_{lim} B^m \partial_j B_k, \\
&= \quad -(\delta_l^i \delta_m^k - \delta_m^j \delta_l^k) B^m \partial_j B_k, \\
&= \quad (\vec{B}.\vec{\nabla})\vec{B} - \vec{B}.(\vec{\nabla}\vec{B}), \\
&= \quad (\vec{B}.\vec{\nabla})\vec{B} - \frac{1}{2}\vec{\nabla} B^2.
\end{aligned}
$$

23

Substituting, the value in eq.(1.31) we will have

$$\rho_m \left(\frac{\partial \vec{v}}{\partial t} \right) = \frac{1}{4\pi} \left[\left(\vec{B}.\vec{\nabla} \right) \vec{B} - \frac{1}{2} \vec{\nabla} B^2 \right] - \rho_q \vec{\nabla} \phi - \vec{\nabla} P, \tag{1.32}$$

where, ϕ is the gravitational potential. In tensor form the above equation can be written as

$$\rho \left(\frac{dv_i}{dt} \right) = - \left(\frac{\partial}{\partial x_i} \right) \left[P + \frac{B^2}{8\pi} \right] + \frac{1}{4\pi} \frac{\partial}{\partial x_i} (B_j B_k) - \rho \frac{\partial \phi}{\partial x_i}. \tag{1.33}$$

As,

$$\frac{d}{dt} = \frac{\partial}{\partial t} + v_j \frac{\partial}{\partial x_j}. \tag{1.34}$$

Putting eq.(1.34) in eq.(1.33) we will get

$$\rho \left[\frac{\partial v_i}{\partial t} + v_j \frac{\partial v_i}{\partial x_j} \right] = - \left(\frac{\partial}{\partial x_i} \right) \left[P + \frac{B^2}{8\pi} \right] + \frac{1}{4\pi} \frac{\partial}{\partial x_i} (B_j B_k) - \rho \frac{\partial \phi}{\partial x_i}. \tag{1.35}$$

The gravitational potential is

$$\phi(r) = -G \int_V \frac{\rho(r')}{|r - r'|} \, d^3 r', \tag{1.36}$$

or

$$\Phi = \frac{-G}{2} \int_V \frac{\rho(r')\rho(r)}{|r - r'|} d^3 r' \, d^3 r, \tag{1.37}$$

writing eq. 1.36 and eq.(1.37) in tensor form we will have

$$\phi_{ik} = -G \int_V \frac{\rho(r')}{|r - r'|} (x_i - x'_i)(x_k - x'_k) \, d^3 r', \tag{1.38}$$

and

$$\Phi_{ik} = \frac{-G}{2} \int_V \frac{\rho(r')\rho(r)}{|r - r'|} (x_i - x'_i)(x_k - x'_k) \, d^3 r' \, d^3 r, \tag{1.39}$$

we can see easily from the above eq.(1.39) that the gravitational potential energy is symmetric i.e; $\Phi_{ik} = \Phi_{ki}$ which yields that

$$\Phi_{ik} = \Phi_{ki} = \frac{1}{2} \int_V \rho(r)(x_k - x'_k) \, d^3 r = \frac{1}{2} \int_V \rho(r)(x_i - x'_i) \, d^3 r. \tag{1.40}$$

Now, the kinetic energy is given by

$$K_{ik} = \frac{1}{2} \int_V \rho v_i v_k \, d^3 r,$$

the magnetic energy is

$$M_{ik} = \frac{1}{8\pi} \int_V B_i B_k \ d^3r,$$

and the inertia of the system is given as

$$I_{ik} = \int_V \rho x_i x_k \ d^3r.$$

From eq.(1.35) we have

$$\rho \frac{d^2 x_i}{dt^2} = - \left(\frac{\partial}{\partial x_i} \right) \left[P + \frac{B^2}{8 \ \pi} \right]$$
$$+ \frac{1}{4 \ \pi} \frac{\partial}{\partial x_i} (B_j \ B_k) - \rho \frac{\partial \phi}{\partial x_i} , \qquad (1.41)$$

multiplying both sides by x_k and integrating over the whole volume we will get

$$\int_V \rho x_k \frac{d^2 x_i}{dt^2} \ d^3r = - \int_V x_k \left(\frac{\partial}{\partial x_i} \right) \left[P + \frac{B^2}{8\pi} \right] d^3r$$
$$+ \int_V x_k \frac{1}{4\pi} \frac{\partial}{\partial x_i} (B_j B_k) \ d^3r - \int_V x_k \rho \frac{\partial \phi}{\partial x_i} \ d^3r. \qquad (1.42)$$

The right hand side of eq.(1.42) will give

$$\int_V \rho x_k \frac{d^2 x_i}{dt^2} \ d^3r = \int_V \rho \frac{d}{dt} \left(x_k \frac{dx_i}{dt} \right) \ d^3r - 2K_{ik}, \qquad (1.43)$$

and the 1st term on the right hand side of eq.(1.42) gives

$$- \int_V x_k \left(\frac{\partial}{\partial x_i} \right) \left[P + \frac{B^2}{8\pi} \right] \ d^3r = - \int_S x_k \rho \left(P + \frac{B^2}{8\pi} \right) \ dS_i$$
$$+ \delta_{ik} \left[\int_V P \ d^3r + \int_V \frac{B^2}{8\pi} \ d^3r \right], \qquad (1.44)$$

or

$$- \int_V x_k \left(\frac{\partial}{\partial x_i} \right) \left[P + \frac{B^2}{8\pi} \right] \ d^3r = - \int x_k \rho \left[P + \frac{B^2}{8\pi} \right] \ dS_i + \delta_{ik} \left[(\gamma - 1) U + \mu \right], \quad (1.45)$$

where, μ is the magnetic field strength, and γ is a constant factor, which is the ratio of two principle specific heat. By substituting, all the values, eq.(1.42) will become

$$\int_V \frac{d}{dt} \left(x_k \frac{dx_i}{dt} \right) \ d^3r = 2K_{ik} + \Phi_{ik} - 2M_{ik} - \int_S x_k \rho \left(P + \frac{B^2}{8\pi} \right) \ dS_i$$
$$+ \frac{1}{4\pi} \int x_k B_i Bj \ dS_j + \delta_{ik} \left[(\gamma - 1) U + \mu \right]. \qquad (1.46)$$

25

We have to decide about the surface integrals. The magnetic field of the system does not vanish at natural boundary of the system, it vanishes when we consider the system, enclosing the whole space in which the magnetic field extends. Since, the magnetic field provides a physical connection between the system proper, and system internal to it. So, it vanishes. Then eq.(1.46) will become magnetic field free and is written as

$$\int_V \frac{d}{dt}\left(x_k \frac{dx_i}{dt}\right)\, d^3r = 2K_{ik} + \Phi_{ik} - 2M_{ik} + \delta_{ik}\left[(\gamma - 1)U + \mu\right]. \qquad (1.47)$$

Since, the right hand side is symmetric so the left hand side should also be symmetric and by using the mass conservation $d/dt \int_V \rho\, d^3r = 0$, eq.(1.47) will become

$$\frac{1}{2}\frac{d^2 I_{ik}}{dt^2} = 2K_{ik} + \Phi_{ik} - 2\,M_{ik} + \delta_{ik}\left[(\gamma - 1)U + \mu\right], \qquad (1.48)$$

contracting the indices we will have

$$\frac{1}{2}\frac{d^2 I}{dt^2} = 2K + \Phi - 2\mu + 3\left[(\gamma - 1)U + \mu\right], \qquad (1.49)$$

for steady state

$$\frac{d^2 I}{dt^2} = 0,$$

hence, we will have

$$2K + \Phi + \mu + 3(\gamma - 1)U = 0. \qquad (1.50)$$

This is the general form of virial theorem which contains magnetic term, kinetic term, potential term, and the internal energy term. For our case, we have neglected the magnetic field, and internal energy so we are left with

$$2K + \Phi = 0. \qquad (1.51)$$

1.7 Doppler Shift in Relativity

We are all familiar with the Doppler effect in acoustics that there is a velocity dependent shift of the sound frequency. If we apply this effect on light, regarding it as a wave, we could also expect a velocity dependent shift of the frequency of light, i.e. there will be

a change in colour due to the relative motion. In sound, the ratio of the observed to the emitted frequency is the sum of the velocities of sound and the object divided by the speed of sound. But in the case of light, we obviously have to deal with the relativistic effects, which are the addition of relativistic velocities and time dilation. What can be done is to use the discovery of Einstein and Planck which relates the energy of light to its frequency.

In 1905, it was already known that the radiation spectrum can easily be understood by regarding the electromagnetic radiation that has been absorbed or emitted by matter in discrete quanta. Einstein predicted the photoelectric effect on the assumption, and this was found to be true. In predicting this he assumed that the energy of a wave-packet of a photon, is proportional to the frequency of light as $E = h\nu$, where, h is called the Planck's constant, and ν is the frequency of the photon.

In order to understand the effect, consider an observer 'A', who is seeing the light emitted from a source 'O' which is moving with a velocity 'v' and the frequency of emitted photons is ν'. Let the motion is along x-axis and, at an instant that the light is emitted, the angle that it makes with the line of sight is θ with the x-axis. The ratio of emitted to the observed frequency is given by [61]

$$\frac{\nu'}{\nu} = \frac{1 - (v/c)\cos\theta}{\sqrt{1 - v^2/c^2}}, \tag{1.52}$$

where c is the speed of light. Its is interesting to consider some special cases. For example, if $\theta = \pi$ then according to eq.(1.52),

$$\frac{\nu'}{\nu} > 1, \tag{1.53}$$

which means that the motion is away from the observer the frequency is decreased. The wavelength and frequency relation is given by

$$\lambda = \frac{c}{\nu}. \tag{1.54}$$

Thus the decrease in frequency increases the wavelength, the shift is called the red-shift. Now if $\theta = 0$ then according to eq.(1.52),

$$\frac{\nu'}{\nu} < 1, \tag{1.55}$$

which means that the motion is towards the observer. This will give a blue-shift. If $\theta = \pi/2$, then the motion is perpendicular to the line of sight there is again a red-shift. This was not expected on classical consideration but had already been observed. The Doppler effect is of great importance, because we can extract a lot of information about the stars. For example, the light emitted from the star that is been observed. Every compound and element in the Universe possesses its own unique spectrum and Doppler effect shifts the entire spectrum.

Chapter 2

The Isothermal Model and Halo Rotational Asymmetry

In Chapter 1, it was explained that the observed temperature asymmetry in the galactic halos is caused by the molecular hydrogen clouds at the CMB temperature [4]. These clouds are populating the galactic halos, and could be detected by the Doppler shift effect emerging due to the rotation of the halos, assuming that the clouds are rotating with the rotating halo [9]. The aim in this chapter is to model these gas clouds and the halo to estimate the rotational asymmetry of the halos of the nearby spiral galaxies (M31, NGC 5128, M33, M81 and M82). Different regions of the halos are modeled by using the three widely adopted dark matter models (NFW, Moore and Burkert model) to get the distribution of the certain number of these gas clouds in that region. This will give us an estimate of the rotational velocity of the halos, and the physical parameters of the gas clouds. Since our cold gas clouds are at the CMB temperature, so they are isothermal. The mass density profile of these clouds can be obtained by using the isothermal Lane-Emden equation, with the condition that the density of the clouds mergers with the density of the ISM at the border. After obtaining the mass density we can constrain the mass, radius and central density of the gas clouds. These gas clouds are called *Bonor-Ebert spheres*. This procedure was first proposed independently by Bonnor [62] and Ebert [63].

The plan of the chapter is as follows: The derivation of the isothermal Lane-Emden equation is given in Section 2.1. Then in Section 2.2, the cold gas clouds are modeled

to estimate their physical parameters. In Section 2.2.1 the total number of clouds in the M31, M33, NGC 5128, M81, and M82 halo is estimated, by using the physical parameters of the gas clouds obtained with the modeling. The filling factor of the cold gas clouds in the M31 halo is estimated in Section 2.2.2. Then in Section 2.2.2 the rotational velocity of the M31 halo is estimated, by assuming that a fraction f of these clouds is present in the galactic halo of M31. In Section 2.2.2 the dynamical mass of M31 halo [64] is used in order to calculate the upper limit of the rotational velocity of the M31 halo. In Section 2.2.3 the upper limit of the rotational velocity of NGC 5128, M33, M81, and M82 halo is also estimated, by using the same procedure used in Section 2.2.2, but using the dynamical mass of these considered galaxies already present in various papers [65, 66, 67, 68].

2.1 The Isothermal Lane-Emden Equation

Consider a spherically symmetric gas cloud at the CMB temperature. Suppose that the cloud is composed of H_2. The equation of hydrostatic equilibrium is given by

$$-\frac{1}{\rho(r)}\nabla P(r) - \nabla \phi(r) = 0. \tag{2.1}$$

Here, $\rho(r)$ is the density of the cloud, $P(r)$ is the pressure applied by the molecules against the gravity, and $\phi(r)$ is the gravitational potential of the system. The equation of state for an ideal isothermal gas is

$$P(r) = \rho(r)c_s^2, \tag{2.2}$$

where, $c_s = (kT_{CMB}/m_H)^{1/2}$, is the isothermal speed of sound, k is the Boltzmann constant, $T_{CMB} = 2.7254^0$K is the CMB temperature, $m_H \approx 3.35 \times 10^{-25}$ g is the mass of single molecule of hydrogen, and $\rho(r)$ is the mass density of the gas cloud. For a pure H_2 cloud, $c_s = 1.36 \times 10^2$ m s^{-1}. Now, the Poisson equation is

$$\nabla^2 \phi(r) = 4\pi G \rho(r), \tag{2.3}$$

where, G is the gravitational constant. From eqs. (2.1) and (2.2)

$$\rho(r) = \rho_{cl} exp\left(-\frac{\phi(r)}{c_s}\right), \tag{2.4}$$

where, ρ_{cl} is the central density of the gas cloud. Eqs. (2.3) and (2.4) can be re-written into the well known Lane-Emden equation for an isothermal cloud, which is given by

$$\frac{1}{\zeta^2}\frac{d}{d\zeta}\left(\zeta^2\frac{d\gamma}{d\zeta}\right) = exp(-\gamma),\tag{2.5}$$

where,

$$\gamma = \frac{\phi(r)}{kT_{CMB}},\tag{2.6}$$

and

$$\zeta = \sqrt{\frac{4\pi G\rho_{cl}}{c_{s_H}^2}}\ r.\tag{2.7}$$

Solving the Lane-Emden equation, with the boundary condition that $\gamma(\zeta = 0) = 0$ and $(d\gamma/d\zeta)|_{\zeta=0} = 0$. The density distribution for a cold gas cloud is given by the relation

$$\rho(r) = \rho_{cl}\ e^{-\gamma}\ .\tag{2.8}$$

Now the total mass of the cloud can be calculated as

$$M_{cl} = \int_0^{R_{cl}} 4\pi\rho(r)r^2\ dr.\tag{2.9}$$

Here, R_{cl} is the radius of the cloud, where it merges with the density of the ISM density. Now, from eqs. (2.7), (2.8) and (2.9) we have the mass of the cloud as

$$M_{cl} = \frac{c_s^3}{(4\pi G^3\rho_{cl})^{\frac{1}{2}}}\int_0^{\zeta_o}\zeta^2 e^{-\gamma}\ d\zeta.\tag{2.10}$$

Here, ζ_o is the dimensionless radius at the boundary of the cloud $\zeta(r = R_{cl}) \to \zeta_o$.

2.2   The Isothermal Lane-Emden Model

Assuming that some fraction, f, of the galactic halo dark matter is composed of a number of our cold gas clouds at the CMB temperature.

It is well known that galactic halos, contain a non-negligible fraction of **hot ionized gas**, which is a source of X-rays. However, estimating the total amount of this hot

31

gas in our and other galaxies is often an open question. An important step forward to try addressing this issue for our Galactic halo has been made recently by Gupta and Mathur [69], who have analyzed Chandra observatory data and find emission and absorption lines towards several active galactic nuclei (AGNs). These lines indicated that the Milky Way halo extends at least up to 139 kpc. Assuming that the M31 halo is similar to that around the Milky Way, and by using, "Table 1", in [70] to estimate the typical hot gas number density in the halos.
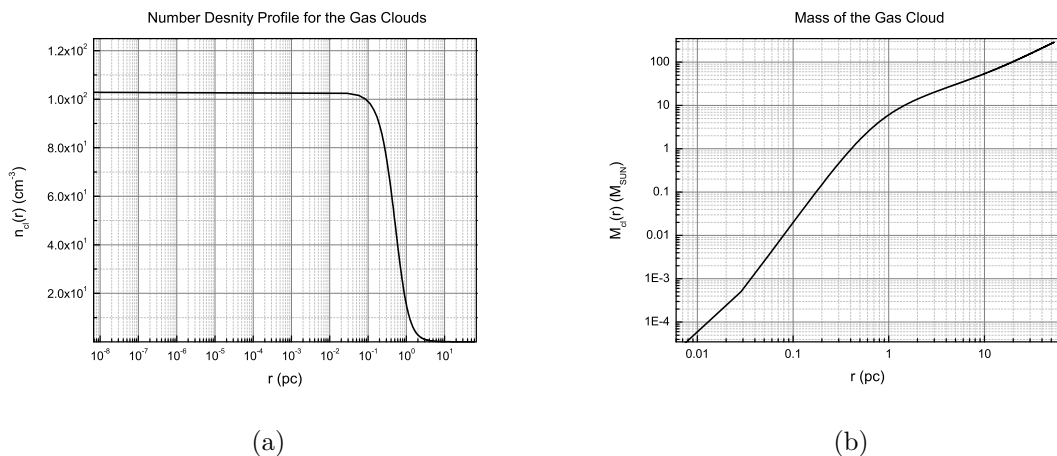
Figure 2.1: Fig. (a) gives the number density profile and Fig. (b) gives the mass profile respectively. Here, the central number density is assumed to be $n_{cl} \simeq 1.0 \times 10^2$ cm^{-3} and the radial distance is given in pc. The external gas density is $\simeq 10^{-2}$ cm^{-3}. The total radius of the cloud is 47 pc.

Table 2.1 gives the central density and radius for each halo model, the number density of ISM to the number density of each cloud n_{ISM}/n_{cl}, the mass, and radius of a single gas cloud, for the considered spiral galaxies (M31, NGC 5128, M33, M81, and M82). Interestingly, from the isothermal Lane-Emden model, one infers that of the gas clouds have a temperature of CMB, their mass by using eqs. (2.9) and (2.10) is always $M_{cl} \simeq 300 \ M_{\odot}$, irrespective of their central density, having radius $R_{cl} \simeq$ 47 pc. Assuming that the ratio, n_{ISM}/n_{cl}, change then we will try to constrain n_{cl} and consequently, r_{cl}, which is the radius of the gas cloud up to which the clouds are optically thick, from *Planck Data*. For illustrative purposes the gas density profile

within the cloud by solving the isothermal Lane-Emden equation (see Appendix A for the Fortran program for the solution of isothermal Lane-Emden equation) is shown in Fig.2.1(a), and the total mass of the gas cloud is shown in Fig.2.1(b). As one can see that the cloud number density is a decreasing function of the radial distance while the mass increases up to R_{cl}.

Table 2.1: Physical parameters of the considered nearby spiral galaxies

Galaxies	Models	ρ_c (g cm^{-3})	r_c (kpc)	n_{cl}/n_{ISM}	M_{dyn} ($10^{10}\ M_\odot$)	M_{cl} $M_\odot$
M31	NFW	2.65×10^{-24}	16.5	10^2	500	300
	Moore	3.20×10^{-25}	31.0	10^2	500	
	Burkert	5.0×10^{-24}	9.06	10^2	500	
NGC 5128	NFW	1.61×10^{-25}	21	10^5	40	299.5
	Moore	4.40×10^{-25}	12	10^5	40	
	Burkert	1.0×10^{-24}	9.8	10^5	40	
M33	NFW	7.0×10^{-25}	35.0	10^5	80	299.5
	Moore	7.64×10^{-26}	18.0	10^5	80	
	Burkert	5.0×10^{-25}	12.0	10^5	80	
M81	NFW	5.10×10^{-24}	10	10^6	200	298.7
	Moore	7.65×10^{-25}	18	10^6	200	
	Burkert	3.68×10^{-24}	8.9	10^6	200	
M82	NFW	4.0×10^{-27}	11	10^6	0.2	298.7
	Moore	1.79×10^{-27}	13	10^6	0.2	
	Burkert	6.29×10^{-27}	9.0	10^6	0.2	

The central density ρ_c (column 3) in units of g cm^{-3}, the core radius r_c in kpc (column 4), the ratio of the central number density of the gas cloud $n_{cl} \simeq 1 \times 10^2$cm^{-3} to the number density of the ISM in the particular galaxy (column 5), the dynamical mass of each galaxy already present in different papers for M31 [64], NGC 5128 [65], M33 [66], M81 [67], and M82 [68] (column 6) is given and the mass of each gas cloud (column 7), are given for all the considered galaxies.

2.2.1 Cloud Distribution in the Halos

In the following section three different models the NFW, Moore and Burkert model already discussed earlier in Chapter 1, Section 1.4 are adopted to describe the gas cloud distribution. It is clear from eqs.(1.5), (1.6), and (1.7) that the first two models are singular towards the center but we are interested in large galatocentric distances. The total number of clouds in the halo is given by the relation

$$N_{Halo} = f \left(\frac{M_{Halo}}{M_{cl}} \right).$$ (2.11)

Here, M_{Halo} is the total mass of the M31 halo, which is given by

$$M_{Halo}(R) = \int_0^R 4\pi r^2 \rho_{N,M,B}(r) \ dr.$$ (2.12)

Here, $R \simeq 200 \ kpc$, is assumed to be the M31 halo size. The total number of the gas clouds in the halo of M31, NGC 5128, M33, M81, and M82 for each halo model (NFW, Moore and Burkert) is shown in Fig.2.2, assuming that the whole halo is made of these cold gas clouds i.e. $f = 1$.

2.2.2 The Halo Rotational Velocity of the M31

In this section, the rotational velocity of the M31 halo is estimated by two methods: by using the filling factor of the cold gas clouds in the halo, and by using the dynamical mass of the galaxy, with the aim to estimate the rotational asymmetry of the halo.

Using the Filling Factor

The filling factor of the gas clouds in the galactic halo of the M31 halo is estimated. The cloud filling factor, S, by the relation

$$S = \begin{cases} N_{Halo} \left(\frac{r_{cl}}{R_{Halo}} \right)^2 & \text{if } S < 1 \ , \\ 1 & \text{if } S \geq 1 \ , \end{cases}$$

where, R_{Halo} is the radius of the halo, N_{Halo} is the number of clouds within the specific radius R_{Halo}, and r_{cl} is the radius of a single gas cloud, which depends upon the central
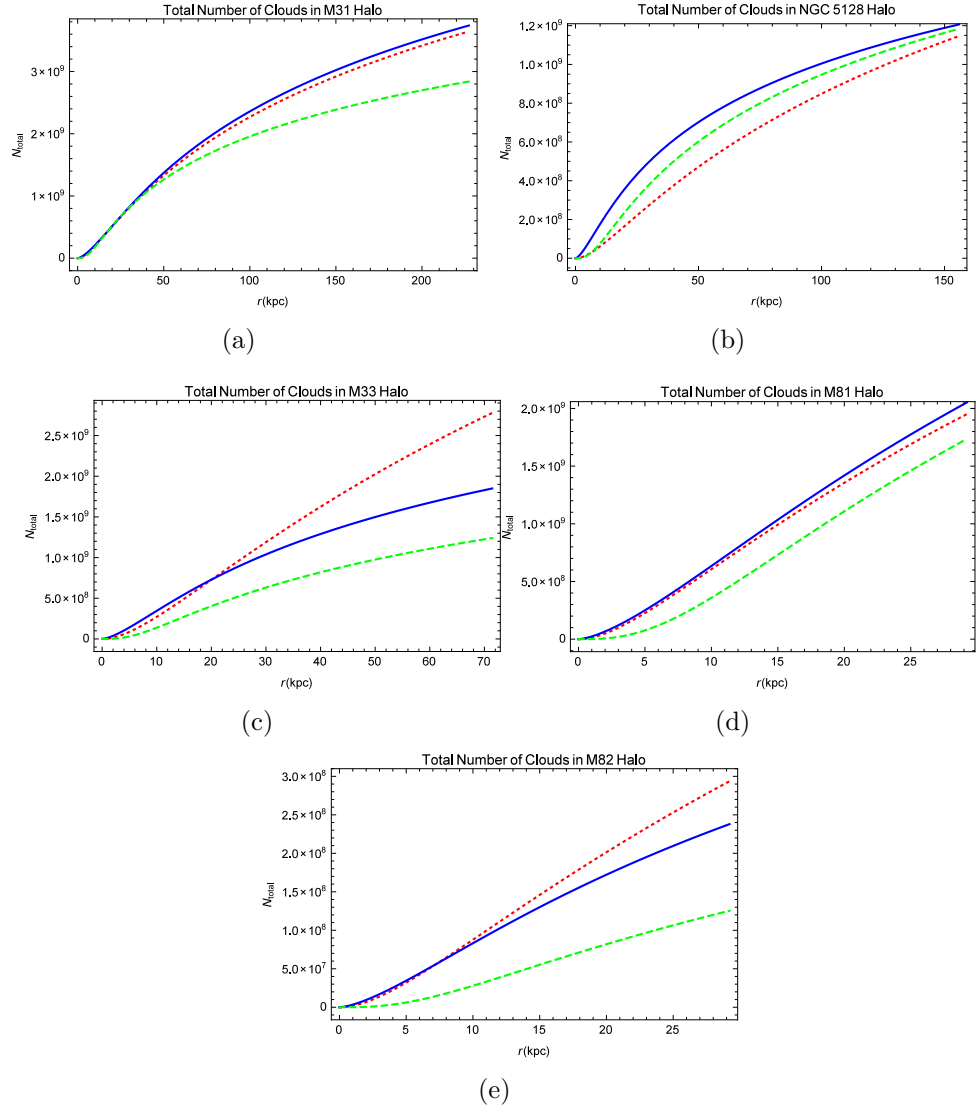
Figure 2.2: The curves in the figure represent the total number of gas clouds in the galactic halo, with the assumption that the total halo of the galaxy is composed of these clouds i.e. $f = 1$. The red-dotted, blue-bold, and green-dashed, represents N_{total} for NFW, Moore and Burkert models. and Fig. (a) gives the total number of clouds in M31 within 200 kpc; Fig. (b) gives the total number of gas clouds in NGC 5128 within 150 kpc; Fig. (c) gives the total number of gas clouds in M33 within 70 kpc; Fig. (d) gives the total number of gas clouds in M81 within 25 kpc; and Fig. (e) gives the total number of gas clouds in M82 within 25 kpc.

density, from Fig.2.1(a) one can see that the cloud density is approximately constant up to a radius about $\simeq 0.3$ pc and then decreases rapidly. By assuming that the cloud has $\bar{\tau} \sim 1$ up to $\simeq 0.3$pc, where, $r_{cl} = c_s/(4\pi G\rho_{cl})^{1/2}$. The assumption that $\bar{\tau} \sim 1$ is a simplifying assumption, a correct calculation of $\bar{\tau}$ would involve summing up the integrated spectral contribution, of the individual line transitions, in a certain *Planck* band. The number of line transitions in the Planck spectral bands is very high, and depend on the chemical species present in each cloud.

The cloud filling factor is shown, within different M31 halo radii as a function of the cloud central density ρ_{cl}, for the NFW, Moore and Burkert models in Fig.2.3.

The M31 halo rotational velocity is estimated by the relation

$$\mathrm{v_{rot}} \simeq \left(\frac{\Delta T}{T_{CMB}}\right)\left(\frac{c}{\sin i f S\bar{\tau}}\right), \tag{2.13}$$

where, c is the speed of light, $i \simeq 77^o$ is the inclination angle of the M31 rotational axis with respect to the line of sight, f is the fraction of gas clouds, with respect to the total amount of the halo dark matter, and $\bar{\tau}$ is the cloud averaged optical depth, over a detector frequency range, $\nu_1 - \nu_2$, i.e. $\bar{\tau} = \frac{1}{\nu_1 - \nu_2}\int_{\nu_1}^{\nu_2} \tau_\nu \, d\nu$, being $\bar{\tau} = 1$ is the cause of black body emission.

The latest release of Planck data [71] and in particular the foreground corrected SMICA band, not available previously, which shows the lowest contamination by the Galactic foreground is used. Note that the SMICA data is used at a resolution corresponding to $N_{side} = 2048$ in HEALPix scheme [72]. The temperature excess from the latest release of Planck data in SMICA band is shown in the last column of Table2.2 for each considered region. We note that the data show a temperature asymmetry in particular the N2+S2 region with N1+S1 which is consistent, particularly for radii larger than $\simeq 40$kpc with the previous analysis.

Using the Dynamical Mass

The aim is to use the dynamical mass of the M31 galaxy to estimate the cloud properties, and their physical parameters. Assume that

$$\tau_{eff} = fS\bar{\tau} , \tag{2.14}$$

Filling Factor for NFW Model

$S(\rho_c)$

$\rho_c\left(\dfrac{g}{cm^3}\right)$

(a)

Filling Factor for Moore Model

$S(\rho_c)$

$\rho_c\left(\dfrac{g}{cm^3}\right)$

(b)

Filling Factor for Burkert Model

$S(\rho_c)$

$\rho_c\left(\dfrac{g}{cm^3}\right)$

(c)
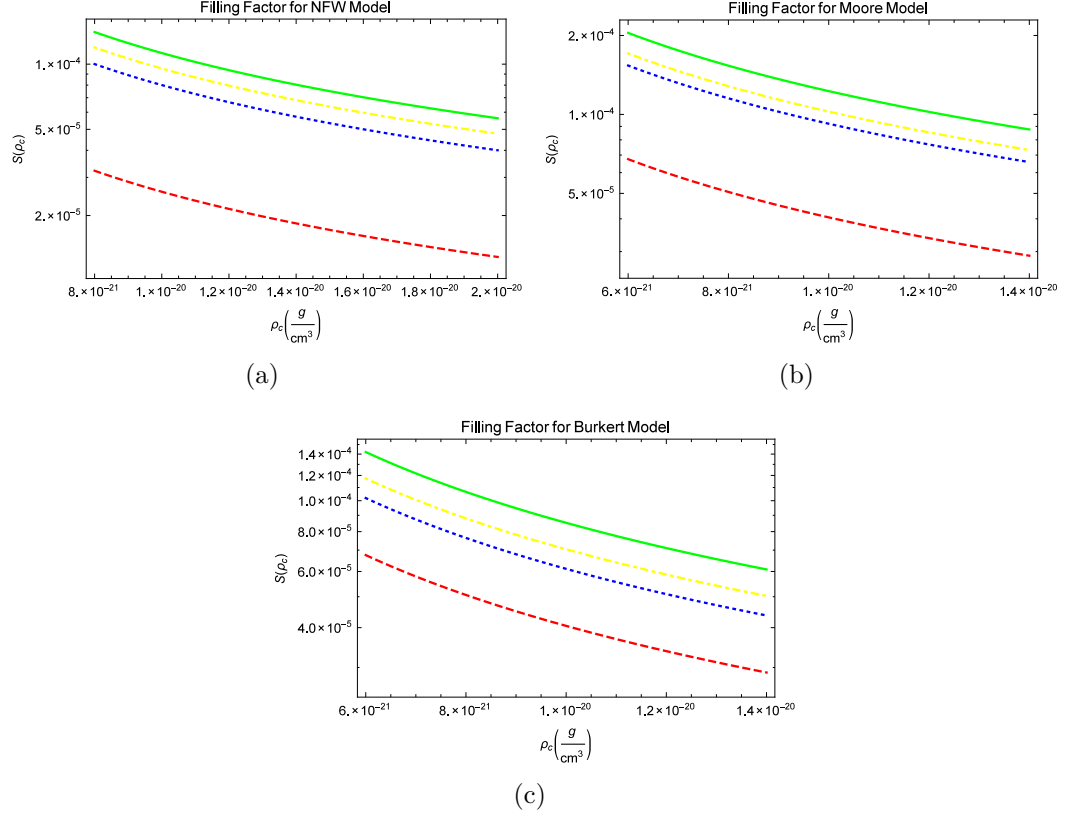
Figure 2.3: Each curve gives the estimated value of the cloud filling factor S for different radii of the M31 halo, with $f = 1$. The dashed, dotted, dash-dotted, and continuous lines corresponds to R_{Halo} values of 41.5 kpc, 51.9 kpc, 77.8 kpc, and 103.8 kpc respectively.

where τ_{eff} is the effective optical depth responsible for the temperature asymmetry, assumed as above that the clouds are at the CMB temperature so that the halo rotational velocity is given by the relation

$$\text{v}_{\text{rot}} = \frac{\Delta T}{T_{CMB}} \frac{c}{2 \sin i \tau_{eff}}. \tag{2.15}$$

The dynamical mass is defined as

$$M_{dyn} = \frac{\text{v}_{\text{rot}}^2 \, R_{Halo}}{G}. \tag{2.16}$$

Eqs.(2.15) and (2.16) entail that

$$M_{dyn}(\leq R_{Halo}) = \left(\frac{R_{Halo}}{G}\right) \left(\frac{\Delta T}{T_{CMB}} \frac{c}{2 \sin i \tau_{eff}}\right)^2. \tag{2.17}$$

Hence,

$$\tau_{eff}(\leq R_{Halo}) \simeq 24.6 \sqrt{\frac{R_{Halo}(\Delta T)^2}{M_{dyn}}}, \qquad (2.18)$$

It is interesting to note that by using the values for f, and S from Table 2.2, and the values for τ_{eff} from Table 2.3, and using eq.(2.14), we can also estimate the average optical depth of the gas clouds which turns out to be $\bar{\tau} \simeq 1$.

Table 2.3: Upper limit of the rotational velocity of the M31 halo

Models	R_{Halo}	M_{dyn}	ΔT	τ_{eff}	v_{rot}
	(kpc)	(10^{12} M$_\odot$)	(μK)	(10^{-3})	(km s^{-1})
NFW	41.5	0.3	17.6	5.1	187
	51.9	0.4	39.2	12.0	182
	77.8	0.5	21.7	6.7	176
	103.8	0.7	21.4	6.9	170
Moore	41.5	0.3	17.6	5.1	188
	51.9	0.4	39.2	11.8	186
	77.8	0.5	21.7	6.5	180
	103.8	0.7	21.4	6.7	172
Burkert	41.5	0.3	17.6	5.2	183
	51.9	0.4	39.2	12.4	177
	77.8	0.5	21.7	7.1	170
	103.8	0.6	21.4	7.4	168

For each M31 halo model indicated in the first column and within the radii in column 2 we give the M31 dynamical mass (column 3) and the temperature asymmetry (in μK) obtained by SMICA data. We then derive the cloud effective optical depth τ_{eff} (column 5) and the M31 halo rotational velocity (column 6) by using eqs. (2.15) and (2.18), respectively.

2.2.3 Halo Rotational Velocity of other Spiral Galaxies

We have the upper limit for the rotational velocity of the M31 halo. We can use the same procedure to calculate the upper limit of the rotational velocity for other spiral

galaxies (NGC 5128, M33, M81, and M82). The dynamical mass of the galaxies, mass of the gas clouds in the galaxies and the ratio n_{cl}/n_{IM} is shown in Table 2.1. In Table 2.4, the values of the effective optical depth by using eq.(2.18), the angle of inclination from the line of sight i, and the corresponding halo rotational velocity v_{rot}[1] are shown.

In the case of NGC 5128 v_{rot} is in the range $15 - 90$ km s^{-1}, depending strongly on the considered *Planck* band but not varying much with the value of R_{Halo}. In the case of the M33 galaxy, v_{rot} is between 30 km s^{-1} and 150 km s^{-1} and depends strongly on the considered frequency band. For the M81 galaxy v_{rot} turns out to be in the range $250 - 450$ km s^{-1}, while for M82 it is between -100 km s^{-1} and 345 km s^{-1}. In particular, in the case of M82, the halo rotation velocity (which, in our model, is assumed to be fixed and equal to that observed for the galactic disk, that is certainly a simplified assumption) seems to change sign in the outer galactic region, outside about $30 - 60$ kpc from the galactic center. Actually, the signs of a complex behavior of the M82 dynamics were already present in the literature and interpreted as possibly resulting from the interaction of M82 with the M81 and NGC 3077 galaxies in the past [18].

Table 2.4: Estimated effective optical depth and halo rotational velocity of the considered galaxies

Galaxies	i	Frequency (GHz)	R_{Halo} (kpc)	ΔT (μK)	τ_{eff} (10^{-3})	v_{rot} (km s^{-1})
NGC 5128	14.6^0	70	92	70	4.80	89
			171	32	4.43	83
			245	12	4.40	74
		100	92	60	4.46	41
			171	42	5.11	53
			245	18	5.35	58
		143	92	58	3.27	15
			171	46	4.00	23
			245	19.5	4.17	24

Continued on next page

[1]Note that the data published in the literature for the various galaxies [15, 16, 17, 18] in the 70 GHz, 100 GHz, and 143 GHz bands at resolution corresponding to $N_{side} = 2048$ in HEALPix scheme [72] is used. The temperature excesses are shown in Table2.2.3 (column 4).

Galaxies	i	Frequency (GHz)	R_{Halo} (kpc)	ΔT (μK)	τ_{eff} (10^{-3})	v_{rot} (km s^{-1})
M33	59^0	70	92	70	4.05	150
			171	30	3.78	139
			245	14	3.71	125
		100	92	60	3.61	64
			171	42	4.28	90
			245	18	4.48	98
		143	92	58.5	2.96	30
			171	46	3.25	38
			245	19.5	3.49	41
M81	14^0	70	15	55.5	1.10	312
			30	65	0.93	265
			60	80	0.99	253
		100	15	40	1.66	366
			30	55	1.55	310
			60	75	1.47	281
		143	15	45	2.64	451
			30	50	2.56	422
			60	75	2.56	422
M82	26^0	70	15	49.5	10.1	286
			30	42.5	13.1	244
			60	-16	11.4	-92
		100	15	46	9.68	275
			30	48	14.0	276
			60	-18	12.1	-103
		143	15	60	11.0	345
			30	60	15.6	346
			60	-12	9.9	-69

For the considered galaxies we give the inclination angle i of the rotation axis with respect to the line of sight (column 2), the central frequency of the considered *Planck* band (column 3), the corresponding radius of the halo R_{Halo} (column 4) within which the temperature asymmetry ΔT (column 5) is detected. In column 6 and 7, τ_{eff} and the corresponding value of the halo rotational velocity v_{rot} is shown.

Table 2.2: Estimated rotational velocity of the M31 halo

Models	R_{Halo}	N_{Halo}	ρ_{cl}	r_{cl}	f	S	$\dfrac{\Delta T}{T_{CMB}}$	v_{rot}
	(kpc)	(10^9)	$(10^{-22}$ g cm$^{-3})$	(pc)		(10^{-2})	(10^{-6})	(km s^{-1})
NFW	41.4	0.8	3.6	0.3	1	2.7	6.4	34
			2.6	0.2		3.8		25
	51.9	1.1	3.6	0.3	1	1.9	14.3	107
			2.6	0.2		2.7		78
	77.8	1.6	3.6	0.3	1	1.3	7.9	89
			2.6	0.2		1.8		64
	103.8	2.1	3.6	0.3	1	0.9	7.8	128
			2.6	0.2		1.2		92
Moore	41.4	0.8	3.6	0.3	1	2.8	6.4	33
			2.6	0.2		3.9		24
	51.9	1.1	3.6	0.3	1	2.0	14.3	107
			2.6	0.2		2.8		75
	77.8	1.6	3.6	0.3	1	1.3	7.9	85
			2.6	0.2		1.9		62
	103.8	2.1	3.6	0.3	1	0.9	7.8	123
			2.6	0.2		1.3		89
Burkert	41.4	0.7	3.6	0.3	1	2.7	6.4	35
			2.6	0.2		3.7		25
	51.9	0.9	3.6	0.3	1	1.8	14.3	115
			2.6	0.2		2.5		83
	77.8	1.2	3.6	0.3	1	1.1	7.9	99
			2.6	0.2		1.6		72
	103.8	1.9	3.6	0.3	1	0.7	7.8	149
			2.6	0.2		1.0		107

For each halo model, I give the estimated cloud filling factor with in the specified R_{Halo} values (column 7) and corresponding estimated rotational velocity of the M31 halo (column 9). We also give the number of the gas clouds in the M31 halo for each radius (column 3). In column 4 and 5, I give the central density for the clouds and the corresponding radius. The value $f = 1$ has been assumed.

Chapter 3

The Virial Model

In the previous chapter we have modeled the cold gas clouds and the galactic halos of the nearby galaxies by using three different models NFW, Moore and Burkert model (explained in Section 2.2.2), in order to estimate the physical parameters of these clouds and also the rotational velocity of the galactic halos of the nearby spiral galaxies (explained in Section 2.2.2, 2.2.3). It was seen that the cold gas clouds provide a good estimation of the rotational asymmetry of the galactic halos. The estimated rotational velocities were more or less equal to the values obtained observationally. It is now known that the cold gas clouds are formed corresponding the viral theorem. So, they are called "virial clouds". It is also seen in Chapter 2 that the density profile of the virial clouds could be given by the solution of the isothermal Lane-Emden equation with the boundary condition that the density should be approximately *zero* at the boundary and merges with the density of ISM. Sir James Jeans had applied the same analysis for the formation of a normal star, he took the boundary condition that the density of the cloud should merge with the density of the ISM. It was called the "*Jeans fiddle*" [73]. In that case the central density had to be put in on an ad-hoc basis. We do not have to do this. Instead of the isothermal Lane-Emden equation, the canonical ensemble distribution is used to obtain the mass density profile of the virial clouds. Since they are formed due to the Jeans instability, we also need to introduce the Jeans mass and radius as giving a definite boundary for the cloud, so that its density distribution is not flat at the border but goes to zero at a definite angle, as the cloud would have

broken away due to a density fluctuation. The aim is to model the virial clouds with the contamination of other interstellar matter, and to see how the physical parameters of these clouds could vary. This is what we are really interested in determining.

The plan of the chapter is as follows: In Section 3.1, the derivation of the Jeans criterion for gravitational collapse is given. Then in Section 3.2, and 3.3, the single-fluid and two-fluid model for the virial clouds are explained.

3.1 Jeans Criterion

Jeans Criterion is named after a British physicist, Sir James Jeans, who considered the process of gravitational collapse, within a gaseous cloud. The condition for equilibrium of a stable, gravitationally bound system is given by the virial theorem (discussed earlier in Chapter 1, Section 1.6) which is given by eq.(1.51). The kinetic energy, K, in the equation is given as

$$K = \frac{3}{2}NkT_{CMB}, \tag{3.1}$$

where, $k = 1.38 \times 10^{-23}$ kgm^{2}s^{-2}K^{-1} is the Boltzmann constant, $T_{CMB} = 2.7254 \ ^0K$ is the CMB temperature, N is the total number of molecules in the cloud. The gravitational potential energy term in the equation, for a cloud with constant central density is, $\phi(R)$, and we need to calculate this term. By definition the gravitational potential energy for a spherically symmetric cloud with radius, R, and total mass, M, is given as

$$\phi(R) = -\int_0^R \frac{GM(r)m}{r} \ dr, \tag{3.2}$$

where, $G = 6.65 \times 10^{-11}$ kg^{-1}m^{3}s^{-2} is the Newton's gravitational constant, m is the mass of single molecule. Now, if the cloud has a constant central density, ρ_c, then the total mass of the cloud is $M(r) = (4/3)\pi\rho_c r^3$. So, eq.(3.2) will take the form

$$\phi(R) = -\int_0^R \frac{4\pi\rho_c G r^2 m}{3} \ dr. \tag{3.3}$$

Solving, eq.(3.3) we will have the gravitational potential energy of a self gravitating, spherically symmetric cloud, and is given by

$$\phi(R) = -\frac{3GM^2}{5R}. \tag{3.4}$$

Putting, K, and $\phi(R)$, in eq.(1.51), we have

$$\frac{1}{2}NkT_{CMB} = \frac{GM^2}{5R}. \tag{3.5}$$

Since, the cloud is collapsing, so, eq.(3.5), will take the form

$$\frac{1}{2}NkT_{CMB} < \frac{GM^2}{5R}. \tag{3.6}$$

Substituting, $N = M/m$, in the above equation we will have

$$\frac{kT_{CMB}}{2m} < \frac{GM}{5R}, \tag{3.7}$$

or,

$$M > \frac{5RkT_{CMB}}{2Gm}. \tag{3.8}$$

The volume of a sphere is $V = (4/3)\pi R^3$, and $V = M/\rho_c$, so, $R = (3M/4\pi\rho_c)^{1/3}$. Substituting, the value of, R, in eq.(3.8), and simplifying it, we will get the total mass of the cloud which is given as

$$M > \left(\frac{1}{2\pi\rho_c}\right)^{1/2} \left(\frac{5kT_{CMB}}{3mG}\right)^{3/2}. \tag{3.9}$$

According to the Jeans criterion the total mass of the cloud should be greater than the Jeans mass, i.e. $M > M_J$ [34], so, eq.(3.9) will give the Jeans mass as

$$M_J^2 \simeq \left(\frac{1}{2\pi\rho_c}\right) \left(\frac{5kT_{CMB}}{3mG}\right)^3. \tag{3.10}$$

From the volume of the sphere we have the corresponding Jeans radius given as

$$R_J = \left(\frac{9kT_{CMB}}{4\pi m\rho_c G}\right)^{1/2}. \tag{3.11}$$

The molecules in the cloud will try to push the gas cloud out, and gravitational force as it is dominating over the motion of these molecules try to compress it due to this motion, we have to introduce the isothermal speed of sound. Since, the kinetic energy is due to the motion of molecules, and the motion due to the molecules and gravity is

44

constrained to be one dimensional, so, $K = (1/2)\gamma kT_{CMB}$, where, γ, is a constant. We have the isothermal speed of sound as

$$c_s = \sqrt{\frac{\gamma kT_{CMB}}{m}}. \tag{3.12}$$

Eqs.(3.10), and (3.11) will take the form

$$M_J^2 \simeq \left(\frac{1}{2\pi\rho_c}\right)\left(\frac{c_s^2}{G}\right)^3, \tag{3.13}$$

and

$$R_J^2 = \frac{27c_s^2}{20\pi\rho_c G}. \tag{3.14}$$

Clearly, from eqs.(3.13), and 3.14, the Jeans mass, and radius, are depending upon the central density of the cloud. So, we need to calculate the central density of the gas cloud to estimate the Jeans mass, and radius, which will be calculated in Section 3.2, and 3.3.

3.2   The Single-Fluid Model

Consider, a spherical cloud of pure molecular hydrogen, each molecule has a mass $m_H \approx 3.35 \times 10^{-27}$ kg, and the total mass of that cloud is M_H. The cloud is allowed to collapse due to the gravitational instability. Since, even the vibrational and the rotational mode is not excited at the CMB temperature, so, they don't vibrate nor rotate at it. Hence, $\gamma = 5/3$, in eq.(3.12), which is the ideal gas approximation. So, $c_s \simeq 1.36 \times 10^2$ m s^{-1} (in this case $m = m_H$). The canonical ensemble distribution is given by eq.(1.11), where, $H(r,p)$ is the Hamiltonian of the system, defined as

$$H(r,p) = p^2/2m + GM(r)m/r, \tag{3.15}$$

where, $p = mc_s$, is the momentum of the molecules. The partition function is defined by eq.(1.12), putting in the Hamiltonian we have the partition function as

$$Z = \frac{1}{h^{3N}N!}\frac{3^{3/2}\pi^{3/2}}{2^{1/2}}\frac{(kT_{CMB})^3}{(G\rho_c)^{3/2}}. \tag{3.16}$$

45

The distribution will become

$$f(r,p) = \frac{2^{1/2}}{3^{3/2}\pi^{3/2}} \frac{(G\rho_c)^{3/2}}{(kT_{CMB})^3} \; exp\left[-\left(\frac{3p^2}{10m^2c_s^2} + \frac{3GM(r)}{5rc_s^2}\right)\right]. \tag{3.17}$$

Now,

$$\rho(r) = \int_{-\infty}^{\infty} 4\pi m p^2 f(r,p)dp. \tag{3.18}$$

By solving eq.(3.18), we have the mass density distribution given by

$$\rho(r) = 8m^{5/2}\left(\frac{G\rho_c}{3k\;T_{CMB}}\right)^{3/2} exp\left(-\frac{3GM(r)}{5rc_s^2}\right), \tag{3.19}$$

where, $M(r)$ is the total mass of the cloud interior to r and is defined as

$$M(r) = \int_0^r 4\pi\rho(q)q^2\;dq. \tag{3.20}$$

The boundary conditions are that the central density is ρ_c and $(d\rho(r)/dr)|_{r\to0} = 0$. Taking natural logarithm of eq.(3.19) and substituting eq.(3.20), we will get

$$\int_0^r 4\pi q^2\rho(q)\;dr = -\left(\frac{rk\;T_{CMB}}{4\pi mG}\right)\ln\left(\frac{\rho(r)}{\zeta}\right), \tag{3.21}$$

where, $\zeta = (8m^{5/2}/3^{3/2})(G\rho_c/k\;T_{CMB})^{3/2}$. Taking the derivative of eq.(3.19) with respect to r, and substituting eq.(3.21). The differential equation is given as

$$r\frac{d\rho(r)}{dr} - r^2\left(\frac{4\pi Gm}{k\;T_{CMB}}\right)\rho^2(r) - \rho(r)\ln\left(\frac{\rho(r)}{\zeta}\right) = 0. \tag{3.22}$$

This is essentially the Lane-Emden equation. We now solve it numerically with a guess value for the central density, and see where the density becomes zero. We then check the value of the Jeans radius with that central density. We then adjust the value of the central density, so that the density becomes zero, exactly at the Jeans radius. In this way, we get a self-consistent solution of the differential equation, subject to the given boundary conditions. The result of the calculation, depicted in Fig. 3.1, yield $\rho_c \simeq 1.60 \times 10^{-18}$ kgm^{-3}, the Jeans Radius, $R_J \simeq 0.32$ pc, and the Jeans mass is $M_J \simeq 0.78\;M_\odot$.
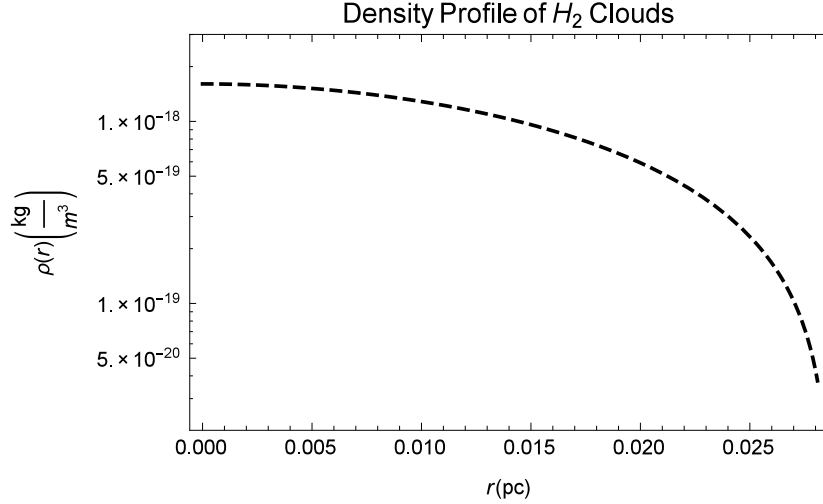
Figure 3.1: The curve represents the density of the virial clouds, assuming that they are only composed of molecular hydrogen. It is clear from the figure that the density of the cloud at the center is $\rho_c \simeq 1.60 \times 10^{-18}$ kgm^{-3}, which is the central density. The density goes on decreasing and is exactly zero at $R_J \simeq 0.32$ pc.

We have estimated physical parameters of the virial clouds, with the assumption that they are pure molecular hydrogen clouds. There is also a possibility that the left over interstellar dust will form another cloud without the contamination of molecular hydrogen.

Assuming that a single dust grain is CN_2O_3, then the mass of a single grain will then be $m_d \approx 1.46 \times 10^{-25}$kg, the total mass of this cloud interior to r. The mass density profile, of these clouds, is shown Fig.3.2. The central density for the dust cloud is $\rho_c \simeq 1.46 \times 10^{-17}$ kgm^{-3}, the Jeans mass is $M_J = 8.98 \times 10^{-4}$ $M_\odot$, and the corresponding Jeans radius, $R_J \simeq 1.40 \times 10^{-3}$ pc. It is clear from Fig.3.1, and Fig.3.2 that the density of the dust cloud is greater than that of pure molecular hydrogen cloud but the Jeans radius is smaller.

3.3 The Two-Fluid Model

As explained earlier, we need to extend our analysis to a mixture of two fluids, hydrogen and dust. The total mass of the cloud will be $M_{cl}(r) = \alpha \ M_H(r) + \beta \ M_d(r)$, where,

Density Profile of Dust Clouds
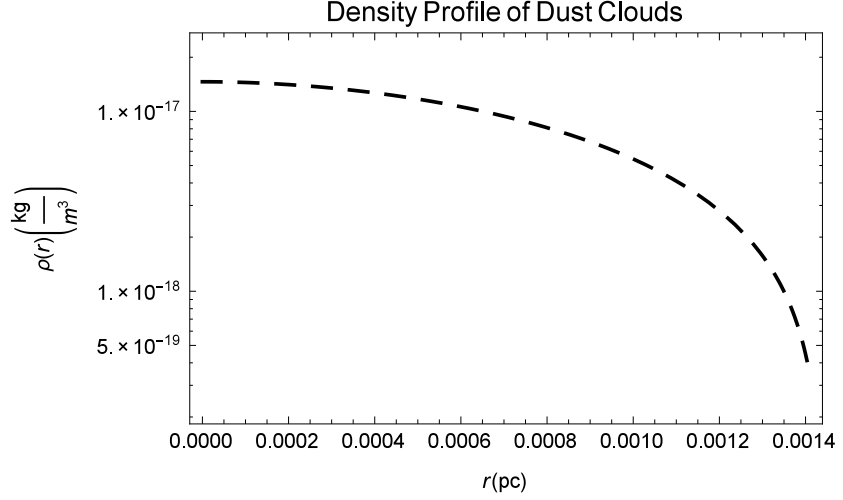
Figure 3.2: The curve represents the density of the dust clouds. It is clear from the figure that the central density of the cloud is $\rho_c \simeq 1.46 \times 10^{-17}$ kgm^{-3}. The density goes on decreasing and is zero at $R_J \simeq 1.40 \times 10^{-3}$ pc.

$M_H(r)$ is the total mass of the molecules of hydrogen, and $M_d(r)$ is the total mass of the dust grains interior to r, where, α and β are the fractions of hydrogen and dust, so that $\alpha + \beta = 1$. Let the mass density of the whole cloud is ρ_{cl}. We have two fluids whose molecules are distinguishable and non reactive. The partition function of the system will be $Z = Z_H.Z_d$, where, Z_H is for hydrogen molecules and Z_d for dust molecules. Similarly, the canonical ensemble distribution will become

$$f(r,p) = \frac{1}{h^{(3N_H+3N_d)} N_H! N_d!} \frac{1}{Z} exp\left(-\left[\frac{H_H(r,p_H)}{kT_{CMB}} + \frac{H_d(r,p_d)}{kT_{CMB}}\right]\right), \qquad (3.23)$$

where, N_H and N_d are total number of molecules of hydrogen and dust, $H_H(r,p_H)$ and $H_d(r,p_d)$ are the Hamiltonian for molecular hydrogen and dust grain clouds. The mass density distribution of the two-fluid model is given by

$$\rho_{cl}(r) = \sqrt{\frac{64}{27}} \frac{(G\rho_{c_H}\rho_{c_d})^{3/2}}{(kT_{CMB})^{9/2}} (m_H m_d)^{5/2} exp\left[-\frac{1}{2}\left(\frac{\alpha GM_H(r)m_H}{rkT_{CMB}} + \frac{\beta GM_d(r)m_d}{rkT_{CMB}}\right)\right],$$
$$(3.24)$$

where, ρ_{c_H}, and ρ_{c_d}, are the central density of the molecular hydrogen and dust cloud. Also

$$\int_0^r \left(\alpha m_H \rho_H(q) + \beta m_d \rho_d(q)\right) q^2 \, dq = -\left(\frac{2rkT_{CMB}}{4\pi G}\right) \ln\left(\frac{\rho_{cl}(r)}{\eta}\right), \qquad (3.25)$$

48

and $\eta = (64/27)^{1/2}[(G\rho_{c_H}\rho_{c_d})^{3/2}/(kT_{CMB})^{9/2}][m_H m_d]^{5/2}$. The differential equation for the two fluid model is

$$r\frac{d\rho_{cl}(r)}{dr} - r^2 \left(\frac{2\pi G}{kT_{CMB}}\right) [\rho_{cl}(r)\,(\alpha\rho_H m_H + \beta\rho_d m_d)] - \rho_{cl}(r)\ln\left(\frac{\rho_{cl}(r)}{\eta}\right) = 0. \quad (3.26)$$

The density distribution, with different fractions of hydrogen and dust, is shown in Fig.3.3. It is seen that with the increase in contamination of dust, the density of virial cloud increases, but the Jeans radius is decreased and so as the corresponding Jeans mass. The Jeans mass, radius, and central density for different fractions, is shown in Table 3.1.
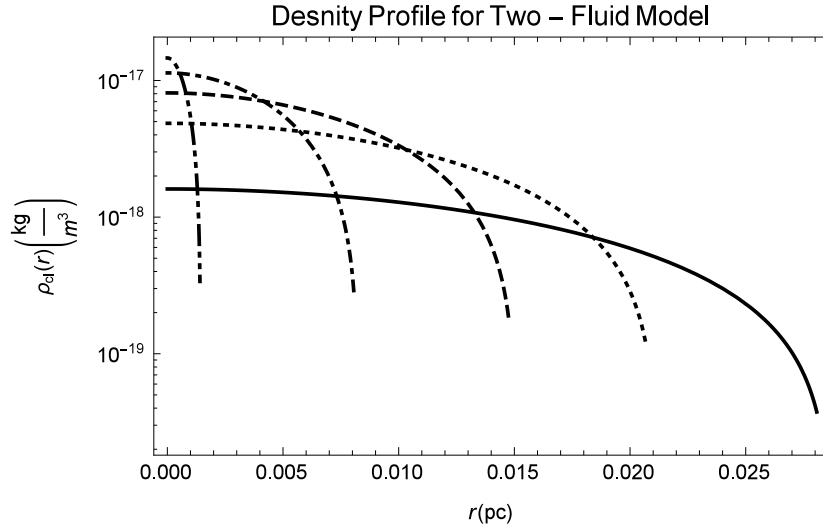
Figure 3.3: The curves in this figure represents the density profile for different values of α and β. The bold black curve represents the density profile when $\alpha = 1$ and $\beta = 0$, dotted represents the density profile when $\alpha = 0.75$ and $\beta = 0.25$, dashed represents the density profile when $\alpha = 0.5$ and $\beta = 0.5$, dotted-dashed represents the density profile when $\alpha = 0.25$ and $\beta = 0.75$, and dot-dot-dashed represents the density profile when $\alpha = 0$ and $\beta = 1$. It is clearly seen that the central density, ρ_c, is different for different concentrations of molecular hydrogen, and interstellar dust. The density of the virial cloud increases with the increase in the concentration of interstellar dust in the cloud and the size of the cloud is decreased.

Table 3.1: Physical parameters for the considered two-fluid model

α	β	Central Density ρ_c(kg m^{-3})	Jeans mass $M_\odot$	Jeans Radius pc
1	0	1.60×10^{-18}	0.78	0.32
0.75	0.25	5.00×10^{-18}	0.58	0.21
0.5	0.5	6.58×10^{-18}	0.39	0.015
0.25	0.75	1.00×10^{-17}	0.19	0.008
0	1	1.46×10^{-17}	0.00089	0.0014

We give the central density ρ_c (column 3), for different fractions of molecular hydrogen, and interstellar dust, and the corresponding Jeans mass (column 4), and Jeans radius (column 5) of the virial clouds.

Chapter 4

Results and Discussion

After mentioning the historical background of Astronomy and how it evolved in the Astrophysics in Chapter 1, I went on to explain that how the Universe was modeled (see Section 1.1). Then in Section 1.2 it is also discussed that how the temperature asymmetry in CMB was detected. In Section 1.3, Section 1.3.1, and Section 1.4 the galaxies and galactic halos, ISM and the dark matter distribution in the galactic halos is explained. In Section 1.6 and 1.7, the virial theorem and Doppler shift in relativity is explained.

In Chapter 2, the cold gas clouds proposed more than a quarter of century ago [9], were modeled using the isothermal Lane-Emden equation. It was seen that the mass comes to be $M_{cl} \simeq 300\ M_\odot$ irrespective of the central density, and the estimated radius was 46pc. The rotational velocities of the galactic halos of various spiral galaxies, including M31, NGC 5128, M33, M81, and M82 was estimated. The obtained results for M31 rotational velocity are shown in Table 2.2, by estimating the filling factor for M31 v_{rot} turned out to be $\simeq 20 - 130$ km s^{-1} (see Table 2.2, column 9). The upper limit of the rotational velocity of the M31 halo, the value of the effective optical depth τ_{eff} by using eq.(2.18) (see column 5 in Table 2.3) is given in Table 2.3. It is seen that the upper limit on v_{rot} turned out to be in the range $160 - 190$ kms^{-1} (see column 6 in Table 2.3). The upper limit of the rotational velocity of NGC 5128, M33, M81, and M82 halos (see Section 2.2.3) is also estimated and the obtained values are given in Table 2.4. For NGC 5128 v_{rot} is in the range $15 - 90\ km\ s^{-1}$, for M33 galaxy

it is in between 30 $km\ s^{-1}$ and 150 $km\ s^{-1}$, for the M81 galaxy it is in the range $250 - 450\ km\ s^{-1}$ while for M82 it is between $-100\ km\ s^{-1}$ and 345 $km\ s^{-1}$. In the case of M82, the halo rotation velocity seems to change sign in the outer galactic region, outside about $30 - 60$ kpc from the galactic center. Actually, the signs of a complex behavior of the M82 dynamics were already present in the literature and interpreted as possibly resulting from the interaction of M82 with the M81 and NGC 3077 galaxies in the past [18]. The obtained values of v_{rot} for all the spiral galaxies appeared to be not very far from the rotation velocity of the galaxy stellar disks.

In Chapter 3, the virial clouds were modeled by using the canonical ensemble distribution. Not only the virial clouds are modeled if they are pure H_2 clouds or pure dust clouds, they are also modeled with different fractions of H_2 and dust in Section 3.3. It was seen that with the contamination of heavier molecules in the clouds the density of the cloud increases (see Fig.3.3), the mass and the size of the cloud decreases. Since more massive particles "pull in" the other molecules more (see Table 3.1).

We have only considered the possibility of the contamination of matter in the clouds (see Chapter 3, Section 3.3). There might be a possibility of the contamination partly coming from the radiation by relatively hot matter sources. This is not incorporated, and should be checked. So, we need detailed modeling of the virial clouds. One thing that also need to be checked is the luminosity of these clouds associated with the observations.

Since, the masses, sizes and densities of the clouds are different, so, there must be some luminosity of the clouds, that could vary with the contamination of matter and radiation. The virial clouds are at the CMB temperature, so all we should see is the CMB Doppler shift. For the M31 disk and halo, it was found that up to about 20^0 (260 kpc) around the M31 center, in the two opposite regions of the M31 disk there was a temperature difference, ΔT, of about 130μK, and it was also seen that similar effect was seen towards, the M31 halo up to 120 kpc from the M31 center with a peak value of about 40μK [14]. We have seen that a single virial cloud has mass $< 1M_\odot$ and radius < 0.4pc. So, at the present level of accuracy of the Planck satellite, it is impossible to see a single cloud in the patch of the sky associated with it. All we can see is a

patch of the sky with a certain number of clouds. Assuming that the clouds rotate with the halo like a rigid body, the patch having a certain number of clouds will be Doppler shifted with the halo. So, if the halo is moving towards us the patch would be blue-shifted and if the halo is moving away from us the patch will be red-shifted. One could try to estimate it and see how it could vary. All these things will be considered separately, later.

The hope is that by constraining the cloud parameters to fit with the observations, we can determine how much baryonic matter is in these virial clouds.

One then also needs to be investigated that how the clouds would have evolved over billions of years, from the time when the CMB temperature was higher than it is now, to the present value. Precisely saying how did the clouds lose energy over this period? this should also be checked.

Appendix A

Fortran Program for Isothermal Lane-Emden Equation

```fortran
Program   LANEEMDEN_SOLVER
implicit real*8(a-h, o-z)
! SETS
Parameter (NVAR=2,NSTEP=10000)
!SETS REQUIRED BY rkdumb.for
Parameter (NMAX=50, NSTPMX=50000)
Dimension x(NSTPMX), y(NMAX, NSTPMX),vstart(NVAR)
Dimension xx(NSTPMX), yy(NMAX, NSTPMX)
Dimension phi(NSTPMX), dphidcsi(NSTPMX),rhorhoc(NSTPMX)
! Common for nLE exponent
COMMON /ELN_COM/ nLE
! OUTPUT FROM rkdumb.for
COMMON /path/ x,y
! SYSTEM OF ODEs IS HERE!
EXTERNAL derivs

print*, '----------------------------------------'
print*, ' LANEEMDEN_SOLVER.FOR                    '
print*, '----------------------------------------'
print*, ' '

! X LIMITS  (DIMENSIONLESS RADIUS LIMITS)

x1= 1d-8
x2= 40050.0d0
h = (x2-x1)/dfloat(NSTEP)
```

```fortran
! Boundary conditions
vstart(1)=0.0d0     ! 1.0
vstart(2)=0.0d0     ! 0.0
! Exponent appearing in the Lane-Emden equation
nLE = 3.5
! stop the integration when rho/rhoc is less than test
test=0.12d-6

! Solve ODE system
call rkdumb(vstart,NVAR,x1,x2,NSTEP,derivs)

! Store results
do i = 1, NSTEP
xx(i)=x(i)
yy(1,i)=y(1,i)      ! Phi(csi)
yy(2,i)=y(2,i)
phi(i) =y(1,i)      ! Phi(csi)
rhorhoc(i)=exp(-yy(1,i))

dphidcsi(i) = 0.0
enddo

! OUTPUT
open(unit=1,file='laneemden_solver.txt')
do i = 1, NSTEP
!x     phi       q
!print*,    xx(i), yy(1,i), yy(2,i)
write(1,*) xx(i), yy(1,i),rhorhoc(i)  !, yy(2,i)
enddo
close(unit=1)
print*, ''
1000 format(1F6.3, 1x, 1F6.4)


! Find border (in ----> xi=xx(in))
rhoc = 1.0
do i = 1, Nstep
rho=rhorhoc(i)               ! Rho/rhoc
print*, i, XX(I), rho
if(rho .le. test) then
```

```fortran
! Stop the integration when rho/rhoc is less than 10^-3
in=i
xi=xx(in)
goto 1123
endif
enddo


1123 continue

print*, 'DIMENSIONLESS Radius(in): ',in, xi

! Find first derivative
call   find_dphidx(h,NSTEP,xx,phi,dphidcsi)

! Dimensionless mass at cloud border
rmass =xi**2*dphidcsi(in)

print*, 'DIMENSIONLESS Mass(in): ',rmass

! THE SOUND SPEED  AT GIVEN TEMPERATURE T
T = 2.7
rmassparticle= 3.d-24
ath = sqrt(1.38d-16* T/(rmassparticle))


!FIX THE CENTRAL DENSITY TO A GIVEN NUMBER  (GRAM/CM^3)
rhoc= 8.5527616258220896E-020   !1500*3.06d-21! cgs
c        RMASSCLOUD=0.1     ! SOLAR MASSES


c       rhoc=((((rmass*ath**3)/(RMASSCLOUD*2d33))/
c      &   ((4.*3.141592)**0.5*(6.67d-8)**1.5)))**2

rhoism=0.01*1d-24


print*, 'rc, ath'
print*,rhoc, ath,rhoc*test,rhoc*test/rhoism
```

```fortran
            rhoR=rhoc*test

            rMR = rmass*ath**3/((4.*3.141592)**0.5*(6.67d-8)
            **1.5*rhoc**0.5)

            print*, 'PhysMass (solar masses)', rMr/2.d33

            rr= xi*ath/(4*3.141592*6.67d-8*rhoc)**0.5
            print*, 'PhysR (pc)', rr/3.d18


            rc= rr*sqrt(rhoR/(rhoc))
            print*, 'rc: ',rc/3.d18




            ! OUTPUT
            rrconst =(ath/(4*3.141592*6.67d-8*rhoc)**0.5)/3.d18
!pc
            rhoconst=rhoc
!g/cm^3
            rmassconst=(ath**3/((4.*3.141592)**0.5
            &            *(6.67d-8)**1.5*rhoc**0.5))/2.d33    ! msol

            ! Density profile
            open(unit=1,file='phis_solution.txt')
            do i = 1, NSTEP
            write(1,*) xx(i)*rrconst, rhorhoc(i)*rhoconst
            enddo
            close(unit=1)


            ! Mass profile
            open(unit=1,file='mass_vs_radius.txt')
            do i = 1, in+1
            rmass_i =xx(i)**2*dphidcsi(i)*rmassconst
            write(1,*) xx(i)*rrconst, rmass_i
            enddo
            close(unit=1)
```

```fortran
      print*, '...that s all folks.'

      end
cccccccccccccccccccccccccccccccccccccccccccccccccccccccc
c     Functions and Subroutines
c
c
c
cccccccccccccccccccccccccccccccccccccccccccccccccccccccc
c     Find the first derivative d phi /d csi
c
c
c
cccccccccccccccccccccccccccccccccccccccccccccccccccccccc
      SUBROUTINE find_dphidx(h,NSTEP,xx,phi,dphidcsi)
      implicit real*8(a-h, o-z)
      REAL*8 xx(*),phi(*), dphidcsi(*)

! For all points from the second to the second last
      do i = 2, NSTEP -1
      dphidcsi(i) = (phi(i+1) - phi(i-1))/(2.0*h)
      enddo
! First point
      dphidcsi(1) = (phi(2) - phi(1))/(h)
! Seconda last point
      dphidcsi(NSTEP) = (phi(NSTEP) - phi(NSTEP-1))/(h)


      end



cccccccccccccccccccccccccccccccccccccccccccccccccccccc
c
c     SET OF ODEs FOR THE LANE EMDEN
c
c     y1 --> phi
c     y2 --> q
c
c     dydx(1)--> dphi/dx
c     dydx(2)--> dq/dx
```

```fortran
c
cccccccccccccccccccccccccccccccccccccccccccc
      SUBROUTINE derivs(x,y,dydx)
      REAL*8 x,y(*),dydx(*)
      COMMON /ELN_COM/ nLE

! ORDINARY LANE EMDEN
c       ! Equation 1 of the Lane Emden ODE set
c       dydx(1)=y(2) * x**(-2)
c       ! Equation 2 of the Lane Emden ODE set
c       dydx(2)=-(y(1))**nLE * x**(2)

! LANE EMMDEN FOR AN ISOTHERMAL SPHERE
! Equation 1 of the Lane Emden ODE set
dydx(1)=y(2) * x**(-2)
! Equation 2 of the Lane Emden ODE set
dydx(2)=(exp(-y(1))) * x**(2)


      return
      END
cccccccccccccccccccccccccccccccccccccccccccc
      include 'rk4.for'
      include 'rkdumb.for'
```

Bibliography

[1] Bertone, G., "Particle dark matter: observations, models and searches", *Cambridge University Press*, (2010).

[2] Ade, P. A. R., Aghanim, N., Arnaud, M. et al. "Planck 2015 results XIII. Cosmological parameters", *A&A*, **594**, (2016): A13.

[3] De Paolis, F., Ingrosso, G., Jetzer, Ph. et al., "Halo dark clusters of brown dwarfs and molecular clouds", *ApJ*, **500**, (1998): 59-74.

[4] De Paolis, F., Ingrosso, G., Jetzer, Ph. et al. "A scenario for a baryonic dark halo", *A&A*, **295**, (1995): 567-577.

[5] Cen, R., and Ostriker, J. P., "Where are the baryons? II. feedback effects", *ApJ*, **650**, (2006): 560-572.

[6] Fraser-McKelvie, A., Pimbblet, K. A., and Lazendic, J. S., "An estimate of the electron density in filaments of galaxies at z $\sim$ 0.1", *MNRAS*, **415**, (2011): 1961-1966.

[7] Mathur, S., Sivakoff, G. R., Williams, R. J. et al. "On the nature of the z=0 X-ray absorbers: I. Clues from an external group", *IJASS*, **315**, (2008): 93-98.

[8] Revaz, Y., Pfenniger, D., Combes, F. et al. "Simulations of galactic disks including a dark baryonic component", *A&A*, **501**, (2009): 171-187.

[9] De Paolis, F., Ingrosso, G., Jetzer, Ph. et al. "Observing molecular hydrogen clouds and dark massive objects in galactic halos", *A&A*, **299**, (1995): 647-649.

[10] Dixon, D. D., Hartmann, D. H., Kolaczyk, E. D. et al. "Evidence for a galactic gamma-ray halo", *New Astronomy*, **3**, (1998): 539-561.

[11] De Paolis, F., Ingrosso, G., Jetzer, Ph. et al. "A gamma ray Astronomy and baryonic dark matter", *A&A*, **510**, (1999): L103.

[12] Zhezher, Y.V., Nugaev, E.Y. and Rubtsov, G.I., "Probing Milky way's hot gas halo density distribution using the dispersion measure of pulsars", *Astronomy Letters*, **42**, (2016): 173-181.

[13] De Paolis, F., Gurzadyan, V. G., Ingrosso, G. et al. "Possible detection of the M31 rotation in WMAP data", *A&A*, **534**, (2011): L8.

[14] De Paolis, F., Gurzadyan, V. G., Nucita, A.A. et al. "Planck confirmation of the disk and halo rotation of M 31", *A&A*, **565**, (2014): L3.

[15] De Paolis, F., Gurzadyan, V. G., Nucita, A. A. et al. "Planck revealed bulk motion of Centaurus-A lobes", *A&A*, **580**, (2015): L8.

[16] Gurzadyan, V., De Paolis, F., Kashin, A. et al. "Planck view of the M 82 galaxy", *A&A*, **582**, (2015): A77.

[17] De Paolis, F., Gurzadyan, V. G., Nucita, A. A. et al. "Triangulum galaxy viewed by planck", *A&A*, **593**, (2016): A57.

[18] Gurzadyan, V. G., De Paolis, F., Nucita, A. A. et al. "Messier 81's planck view versus its halo mapping", *A&A*, **609**, (2018): A131.

[19] Clive, R., "Essay review: Stonehenge: Neolithic man and the cosmos, by John D. North", *Archaeoastronomy Supplement*, **30**, (1999): S83.

[20] Cajori, F., "Sir Issac Newton's mathematical principles of natural philosophy and his system of the worlds", *University of California Press*, (1947).

[21] Israel, W., "Dark stars: the evolution of an idea", *Three hundred years of gravitation*, (1987): 199-276.

[22] Binney, J. and Michael M., "Galactic astronomy", *Princeton University Press*, (1998).

[23] Einstein, A. "Letter to Willem de Sitter, March 12th" (1917).

[24] O'Raifeartaigh, C., O'Keeffe, M., Nahm, W. et al. "Einstein's 1917 static model of the cosmos: a centennial review", *EPJH* **42**, (2017): 431-474

[25] Friedmann, A., "On the curvature of space", *Zeitschrift fur Physik and translated by Doyle B.*, **10**, (1922): 377-386.

[26] O'Raifeartaigh C. and McCann B., "Einstein's cosmic model of 1931 revisited: an analysis and translation of a forgotten model of the universe ", *The European Physical Journal H*, **39.1**, (2014): 63-85.

[27] Gamow, G., "Expanding universe and the origin of elements", *PR*, **70**, (1946): 572-573.

[28] Gamow, G., "My world line: An informal autobiography" *Viking Press, New York*, (1970).

[29] Hubble, E., "A relation between distance and radial velocity among extra-galactic nebulae", *PNAS*, **15.3**, (1929): 168-173.

[30] Leavitt, H. S., "1777 variables in the magellanic clouds", *AHCA*, **60**, (1908): 87-108.

[31] Einstein, A. "Cosmological considerations on the general theory of relativity", *The Principle of Relativity. Dover Books on Physics*, **240**, (1952): 175-188.

[32] Alpher, R. A., Herman R., "Evolution of the universe", *Nature*, **162**, (1948): 774-755.

[33] Bethe, H. A., "Energy production in stars", *PR*, **55.5**, (1939): 434-456.

[34] Chandrasekhar, S., "An Introduction to stellar structures", *University of Chicago Press*, (1939).

[35] Penzias, A. A., Wilson, R. W., "A measurement of excess antenna temperature at 4080 Mc/s", *ApJ*, **142**, (1965): 419-421.

[36] Dicke, R. H., Peebles, P. J. E., Roll, P. G. et al. "Cosmic black-body radiation", *ApJ*, **142**, (1965): 414-419.

[37] Blumenthal, G. R., Faber, S. M., Primack, J. R. et al. "Formation of galaxies and large-scale structure with cold dark matter", *Nature*, **311**, (1984): 517-525.

[38] NASA, "Understanding the evolution of life in the universe", *NASA WMAP*, (2011).

[39] da Silva, L., and Arany-Prado, L. I., "The age of the galactic thin disk from Th/Eu nucleocosmochronology-III. Extended sample", *A&A*, **440.3**, (2005): 1153-1159.

[40] Amina, H.,"Stellar halos and the link to galaxy formation", *IAU*, **317**, (2016): 228-234.

[41] Elias, L. M., Sales, L. V., Creasey, P. et al. "Stellar halos in illustris: Probing the histories of milky way-mass galaxies", *MNRAS*, **479**, (2018): 4004-4016.

[42] Ralf, S. K., Simon, C. O. G., "Physical processes in the interstellar medium", *Star Formation in Galaxy Evolution: Connecting Numerical Models to Reality, Saas-Fee Advanced Course*, **43**, (2016): 85-249.

[43] Witt, A. N., "The chemical composition of the interstellar medium", *RSLA*, **359**, (2001): 1949-1959.

[44] Ferriere, K., "Structure and components of the interstellar medium", *The Role of the Disk-Halo Interaction in Galaxy Evolution: Outflow vs. Infall? Edited by M.A. de Avillez. EAS Publication Series*, **56**, (2012): 21-29.

[45] Zinnecker, H., Drapatz, S., "Galactic molecular clouds-their size and mass distribution", *IN: Nearby molecular clouds; Proceedings of the Specialized Colloquium, Toulouse, France*, **33**, (1985): A86.

[46] Muzahid, S., Kacprzak, G. G., Charlton, J. C., Churchill, C. W., "Molecular hydrogen absorption from the halo of a $z \sim 0.4$ galaxy", *ApJ*, **823**, (2016): 15-30.

[47] Richter, G., "Molecular hydrogen in the lower galactic halo", *FUSE Proposal*, **ID D008**, (2003).

[48] Solomon, P. M., Sanders, D. B., Scoville, N. Z., "Giant molecular clouds in the galaxy - distribution, mass, size and age", *In: The large-scale characteristics of the galaxy; Proceedings of the Symposium, College Park*, **35**, (1979): A80.

[49] Boruah, M. J., Gogoi, A., Ahmed, G. A., "Laboratory simulation and modeling of size, shape distributed interstellar graphite dust analogues: a comparative study", *Planetary and Space Science*, **125**, (2016): 27-36.

[50] Sterken, V. J., Altobelli, N., Strub, P. et al. "Modeling the local size distribution of interstellar dust in the solar system", *EGU General Assembly*, **22**, (2012): 449.

[51] Witt, A. N., Gordon, K. D., Sell, P. H. et al. "The excitation of extended red emission in interstellar dust", *AAS Meeting 205*, **36**, (2004): 1441.

[52] Rezaei, Kh., Sara, B. J., Coryn, A. L. et al. "Detection of the milky way spiral arms in dust from 3D mapping", *ApJ* (submitted in ApJ 2018): eprint arXiv:1808.00015.

[53] Casuso, E., Beckman, J. E., "Explaining the galactic interstellar dust grain size distribution function", *ApJ*, **139**, (2010): 1406-1410.

[54] Alcock, C., "The MACHO project: microlensing results from 5.7 years of large magellanic cloud observations", *ApJ*, **542**, (2000): 281-307.

[55] Alcock, C., "Binary microlensing events from the MACHO project", *ApJ*, **541**, (2000): 270-271.

[56] Einasto, J., "Kinematics and dynamics of stellar systems", *Astrofiz. Alma-Ata*, **5**, (1965): 87-98.

64

[57] Navarro, J. F., "The structure of cold dark matter halos", *IAU*, **171**, (1996): 255-258.

[58] Moore, B., Quinn, T., Governato, F. et al. "Cold collapse and the core catastrophe", *MNRAS*, **310**, (1999): 1147-1152.

[59] Morse, M. P., "Thermal Physics", *New York Revised Edition*, (1964).

[60] Goldstein, H., Poole, C. P., and Safko, J. L., "Classical mechanics", *Addison Wesley*, (2002)

[61] Qadir, A., "Relativity: An introduction to special theory", *World scientific publishing*, (1989).

[62] Bonnor, W. B., "Boyle's law and gravitational instability", *MNRAS*, **116**, (1956): 351-359.

[63] Ebert, R., "Uber die verdichtung von HI-Gebieten", *Zeitschrift fur Astrophysik*, **37**, (1955): 217-232.

[64] Tamm, A., Tempel, E., Tenjes, P., et al. "Stellar mass map and dark matter distribution in M31", *A& A*, **546**, (2012): A4.

[65] Mathieu, A., Dejonghe, H., and Hui, X., "Probing the halo of centaurus A: A merger dynamical model for the PN population", *A&A*, **309**, (1996): 30-42.

[66] Corbelli, E., "Dark matter and visible baryons in M33", *MNRAS*, **342**, (2003): 199-207.

[67] Oehm, W., Thies, I, and Kroupa, P., "Constraints on the dynamical evolution of the galaxy group M81", *MNRAS*, **467.1**, (2017): 273-289.

[68] Johnny P. G., Paul M., And Todd A. T., "Measurement of the mass and stellar population distribution in M82 with the LBT", *ApJ*, **757**, (2014): 24-30.

[69] Gupta, A., Mathur, S., Krongold, Y. et al. "A huge reservoir of ionized gas around the Milky Way: accounting for the missing mass?" *ApJ*, **756**, (2012): L8.

[70] Zhezher, Y. V., Nugaev, E. Y., and Rubtsov, G.I., "Probing milky way's hot gas halo density distribution using the dispersion measure of pulsars", *AL*, **42**, (2016): 173-181.

[71] Adam, R., Ade, P. A. R., Aghanim, N. et al. (Planck Collaboration), "Planck 2015 results I. Overview of products and scientific results", *A&A*, **594**, (2016): A1.

[72] Gorski, K. M., Hivon, E., Banday, A. J. et al. "HEALPix: A framework for high-resolution discretization and fast analysis of data distributed on the sphere", *ApJ*, **622**, (2005): 759-771.

[73] Jeans, J. H., "The stability of a spherical nebula", *RSL*, **68**, (1901): 454-455.

[74] Tahir, N., De Paolis, F., Qadir, A. et al. "Constraining baryons in the M31 halo using Planck data", *IJMPD*, (2018): (submitted to IJMPD).